19

Zeolites in the Science and Technology of Nitrogen Monoxide Removal

Masakazu Iwamoto
Tokyo Institute of Technology, Yokohama, Japan

Hidenori Yahiro
Ehime University, Matsuyama, Japan

I. INTRODUCTION

A. Relevant Reactions in Environmental Catalysis

The use of catalytic processes in pollution abatement and resource recovery is widespread and of significant economic importance for the realization of sustainable chemistry/industry (1). As has widely been recognized, there are five areas where environmentally benign catalysis would have significant impact:

1. Control of emissions of environmentally unacceptable compounds, especially in flue gases and car exhaust gases
2. Conversion of solid or liquid waste into environmentally acceptable products
3. Selective manufacture of alternative products that can replace environmentally harmful compounds, such as some chlorofluorocarbons (CFCs)
4. Replacement of environmentally hazardous catalysts in existing processes
5. Development of catalysts that enable new technological routes to valuable chemical products without the formation of polluting byproducts

The targets of environmentally benign catalysis lie in air, water, and soil. This chapter will focus primarily on the first topic, that of heterogeneous catalysis for unacceptable materials emitted into the air. This is because the composition and quality of fuels, as well as emission control during fuel utilization, are strongly dependent on the application of heterogeneous catalysis. However, problems and opportunities in water chemistry are also of increasing importance (2–4). The amount of water consumption in industrialized countries is continuously increasing, and in several countries the depletion of underground sources and/or their increasing level of contamination has become of great concern (2). Rational use of water resources is one of key issues for sustainable growth. Although technologies for treating recycled rinse water are available commercially, there are limitations in terms of cost of chemicals/technology, efficiency of removal of pollutants, production of side streams, severity of operation, range of conditions for operation, etc., for which innovative solutions are required. The use of applicable solid catalysts are expected to have significant impact on overcoming or reducing these

limitations, especially in terms of oxidation processes (3) and heterogeneous photocatalysis (4).

Air pollution and acid rain seriously affect terrestrial and aquatic ecosystems, and therefore are very important social problems that require solutions as soon as possible. The exhaust gases from engines of vehicles and industrial boilers contain mainly carbon oxides, nitrogen oxides (NOx), hydrocarbons, sulfur dioxide, particles, and soot. Sulfur compounds produce SOx during combustion in engines and during catalytic regeneration in catalytic cracking units, leading to local contamination and to the poisoning of automotive exhaust catalysts (1,5). Recent research has been conducted in two main areas: (a) development of new catalysts for desulfurization of organic sulfur compounds and (b) development of catalysts capable of reducing SO_2 to elemental sulfur by CO or hydrocarbons.

Particulate matter and NOx are among the main pollutants in diesel engine emissions. The combination of traps and oxidation catalysts appears to be the most plausible posttreatment technique to eliminate soot particles (6). The possibility of promoting both oxidation and NOx reduction in a single catalyst has also been investigated (7). The present status of soot combustion catalysts has been summarized by Querini (8). Fully halogenated CFCs are responsible for the depletion of the ozone layer. The Program for Alternative Fluorocarbon Toxicity Testing has recommended a guide for transforming CFCs into hydrofluorocarbon compounds (HFCs) (9). HFCs show no effect on ozone depletion. To recover CFCs and destroy them is a logical step forward. Many destruction techniques have been proposed (10). Very recently, however, converting CFCs to valuable chemical compounds has been studied as a better choice. This technique involves the selective hydrodechlorination of CFCs to HFCs on supported palladium (11) or nonnoble metals such as nickel (12).

B. Necessity of New DeNOx Technologies

At present, one of the most significant problems in air pollution is the removal of NOx, which is produced during high-temperature combustion. In particular, the removal of nitrogen monoxide (NO) is a dominant target because it is an inert and major component of NOx in exhaust gases (13,14). It is well known that NO is thermodynamically unstable relative to N_2 and O_2 at temperatures below 1200 K. Catalytic decomposition is the simplest and most desirable method for its removal. In the1960s and 1970s, many studies concentrated on the development of catalysts active for the catalytic decomposition of NO, which comprised the "first worldwide research effort for deNOx catalysts." During this period, a few catalysts based on noble metals and metal oxides were reported to be active for NO decomposition; however, a suitable catalyst with sustainable high activity has yet to be found. This is due to the fact that oxygen contained in the feed, or produced in the decomposition of NO, competes with NO for adsorption sites. As a result, high reaction temperatures and/or gaseous reductant is required to remove surface oxygen and regenerate catalytic activity. The catalytic reduction processes employing NH_3, CO, or hydrocarbon reductants on TiO_2(-V_2O_5)-WO_3 or Pt-Pd(-Rh) catalysts have been put to practical use. Much effort has been devoted to improving these reduction processes, but they currently suffer from the following disadvantages or problems:

1. In the selective catalytic reduction system with ammonia (NH_3-SCR), there are several disadvantages, such as high cost of facilities and the use of hazardous ammonia.
2. The automobile catalytic converter is the only technology available for the most stringent emission standards. In this technology, so called three-way catalysts

are preferentially used even though they have limitations such as requiring unleaded gasoline and maintaining a specified air/fuel ratio. However, this system cannot meet the requirements of newly developed engines in which the air/fuel ratio is leaner (air rich) because the exhaust contains a considerable amount of oxygen and the present catalysts do not work under such conditions.

3. The greater use of diesel engine vehicles is a major trend observed worldwide over the last decade. Cogeneration systems using diesel engines have also been under development. Although inherently cleaner than gasoline engines from the viewpoint of CO and hydrocarbons, diesels produce more aldehydes, SOx, NOx, smoke, and odor. In this instance the problem is similar to that above, i.e., removal of NO in the presence of oxygen and SOx remains unsolved.

In 1981 and 1986, Iwamoto and coworkers (13,15) first demonstrated that NO decomposition reaction proceeded over copper ion–exchanged FAU(Y) and MFI zeolites, respectively. Subsequently, Hall et al. (16) confirmed the activity of copper ion–exchanged zeolite. These helped launch another wave of intensive studies, i.e., the "second worldwide research effort for deNOx catalysts."

Later the desire for improved fuel economy and lower carbon dioxide emissions increased the demand for diesel and lean-burn gasoline engines throughout the world. This required the development of catalytic technologies that allow NOx reduction/decomposition in lean conditions, e.g., in oxygen-rich environment (see problem 3 above). In 1990, a breakthrough in NO removal was reported concerning the selective catalytic reduction of NO with hydrocarbons in an oxidizing atmosphere (HC-SCR). This discovery destroyed the widely accepted notion that ammonia was the only selective reductant for NO in the presence of oxygen. This novel HC-SCR process was first reported on copper ion–exchanged zeolites by Iwamoto et al. (17) and by Held et al. (18) independently. The new selective reduction is enhanced remarkably by the presence of oxygen, proceeds even in the presence of water and SO_2, and may eventually override all of the disadvantages of the present reduction systems. Since the discovery of HC-SCR, a vast number of papers dealing with HC-SCR on metal-containing zeolites have been published.

To date, much effort has been devoted to developing new methods for the removal of NO, including decomposition, reduction with hydrocarbons, and adsorption over metal-, metal oxide-, and zeolite-based materials. Future opportunities in the catalytic removal of NO can be classified as follows:

1. Removal of NO without reductant
   a. Adsorption–enrichment–posttreatment
   b. Catalytic decomposition to nitrogen and oxygen molecules
2. Removal of NO with reductant
   HC-SCR in the presence of excess oxygen

This chapter will focus on the results of zeolite-based materials in the order of the processes provided above.

II. REMOVAL OF NO WITHOUT REDUCTANT-ADSORPTION OF NO

A. Amounts of Reversibly and Irreversibly Adsorbed NO on Zeolites

It is widely accepted that selective adsorption is one of the most suitable techniques for removal and/or enrichment of low-concentration pollutants. It is well known that zeolites are good candidates for selective adsorption since they have large surface areas and

uniform window sizes. Three main methods—pressure swing adsorption (PSA), thermal (temperature) swing adsorption (TSA), and pressure-thermal swing adsorption (PTSA)—are used for the removal of pollutants by selective adsorption. PSA has been applied to various processes in practice, such as the enrichment of oxygen in air and the removal of impurities in hydrogen; therefore, PSA is expected to be an effective method for removing or enriching dilute NOx in air. The adsorbents for PSA must possess a high capacity for reversible adsorption of NO; however, little is known of the respective amounts of reversible and irreversible adsorption of NO on metal ion–exchanged zeolites. Iwamoto et al. (19–21) succeeded in the measurement of reversible and irreversible adsorption of NO on metal ion–exchanged zeolites by a fixed-bed flow adsorption apparatus. For discussion of active carbon, carbon fiber, silica, and chelate resins as candidates for NO adsorption, readers are referred to an excellent review (22).

The amounts of reversible and irreversible adsorption of NO per weight of adsorbent (denoted as q_{rev} and q_{irr}, respectively) measured at 273 K on various cation-exchanged MFI zeolites are summarized in Table 1. The values in parentheses are the amounts of reversible and irreversible adsorption of NO per cation (q^*_{rev} and q^*_{irr}). The q_{rev} and q_{irr} changed greatly with the type of metal ion. With MFI zeolites, the order of q_{rev} was transition metal ion $\approx$ alkaline earth metal ion $>$ rare earth metal ion $\approx$ alkali metal ion $\approx$ proton. Among the adsorbents listed in the table, Cu-MFI-157 (metal ion–zeolite structure–exchange level; the exchange level is defined as 100 − [number of cations exchanged] · [valence of cation exchanged] · [number of aluminum atoms in zeolite framework]$^{-1}$; details will be provided in Sec. III.B.1) and Co-MFI-90 showed the largest q_{rev} and q_{irr}, respectively.

The q_{rev} and q_{irr} were also strongly dependent on silica/alumina ratio of the parent zeolites. Note that both q^*_{rev} and q^*_{irr} decreased with zeolite aluminum content, regardless of zeolite structure, as shown in Fig. 1A. Similar results were observed for cozeolites (20) and Ag-zeolites (21). These correlations indicate that the absorption of NO is controlled

Table 1 Adsorption, Decomposition, and Reduction of NO Over Cation-Exchanged ZSM-5 (SiO_2/Al_2O_3 = 23.3) Zeolites

		Adsorption[a]		Decomposition[b]		Reduction[c]		
		Amount of NO adsorbed / cm^3g^{-1}						
Cation	E.L.[d] (%)	q_{rev}(q^*_{rev})	q_{irr}(q^*_{irr})	E.L.[d] %	Conv. to N_2 %	E.L.[d] %	Temp. K	Conv. to N_2 %
Na	100	0.16 (0.006)	0.00 (0.000)	100	0	100	673	0
Ca	54	1.81 (0.246)	1.56 (0.212)	80	0	25	873	12
Sr	105	2.71 (0.159)	0.20 (0.014)					
Cu	157	4.28 (0.206)	14.90 (0.716)	73	79	102	523	41
Co	90	1.52 (0.131)	19.96 (1.693)	80	2	90	673	40
Mn	127	1.19 (0.069)	5.81 (0.339)			127	573	27
Ni	68	1.03 (0.112)	6.64 (0.727)			99	673	38
Fe	62	0.52 (0.061)	3.08 (0.362)	80	0	94	473	12
H	100	0.12 (0.004)	0.32 (0.011)			100	723	39

[a] NO, 1000 ppm; adsorption temp., 273 K; adsorption weight, 0.5 g; flow rate, 100 cm^3min^{-1}; adsorption time, 35 min; desorption time, 60 min.
[b] NO, 1%; temp., 823–825 K; W/F, 4.0 gs cm^{-3}.
[c] NO, 1000 ppm; C_2H_4, 250 ppm; O_2, 2%; W/F, 0.2 $gscm^{-3}$.
[d] Exchange level of cation.

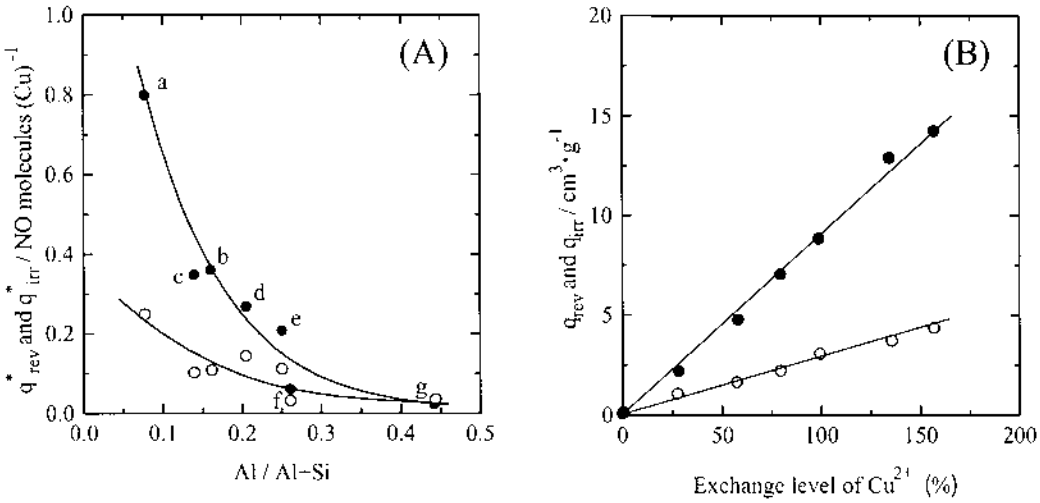

Fig. 1 (A) Change in q^*_{rev} (○) and q^*_{irr} (●) with Al content in the parent zeolites. a, MFI; b, FER; c, MOR; d, OFF/ERI; e, LTL; f, FAU(Y); g, FAU(X). (B) q_{rev} (○) and q_{irr} (●) of Cu-MFI as a function of copper loading. The concentration of NO is 1910 ppm and the adsorption temperature is 273 K. (Reprinted with permission from Ref. 19.)

primarily by the aluminum content and not by the zeolite structure. The fact that the chemical and physical nature of zeolites depends on the aluminum content is well known. For example, acid strengths of proton-exchanged zeolites (23) and the binding energy of each constituent element of the zeolites (24). Consistent with this, the dependence of NO adsorption amount on the aluminum content of zeolite reflects the change in the electronic structure of the zeolite.

The q_{rev} and q_{irr} on MFI zeolite were proportional to the loading of copper ion as shown in Fig. 1B using PSA, showing that a high loading of copper ion into MFI is more favorable for NO removal. Figure 1B demonstrates that the q^*_{rev} and q^*_{irr} of Cu-MFI are constant, approximately 0.23 and 0.64 NO molecule·Cu^{-1}, respectively, and that the effectiveness of each copper ion in the MFI zeolite for NO adsorption is independent of its loading level. Furthermore, the ratio of effective to ineffective Cu ions for NO adsorption is constant (19). On the other hand, in the case of Cu-MOR, q^*_{irr} is constant as the loading of copper ion increases, while q^*_{rev} decreases with increasing copper ion loading. A similar result was observed for Ag-zeolites; both q^*_{rev} and q^*_{irr} of Ag-MFI are constant, while those of Ag-MOR change with the loading of silver ion (21). Thus, the effectiveness of each metal ion for NO reversible adsorption seems to be dependent on zeolite structure, although the adsorptive property of the other types of zeolite should be tested.

Adsorption temperature is an important parameter of PSA determinations. The q_{rev} and q_{irr} clearly depend on the adsorption temperature shown in Fig. 2. With increasing adsorption temperature, q_{irr} on Cu-MFI-157 significantly decreases. On the other hand, q_{rev} gradually increases with temperature, reaches the maximum (4.35 cm^3 g^{-1}) at 243 K, and then decreases. The maximal q_{rev} on Co-MOR-65 was 5.42 cm^3 g^{-1} at 373 K. A high capacity for reversible adsorption of NO is required for PSA. At present, Co-MOR (20) or Ag-MOR (21) are strong candidates for NO adsorbents in high- or low-temperature PSA.

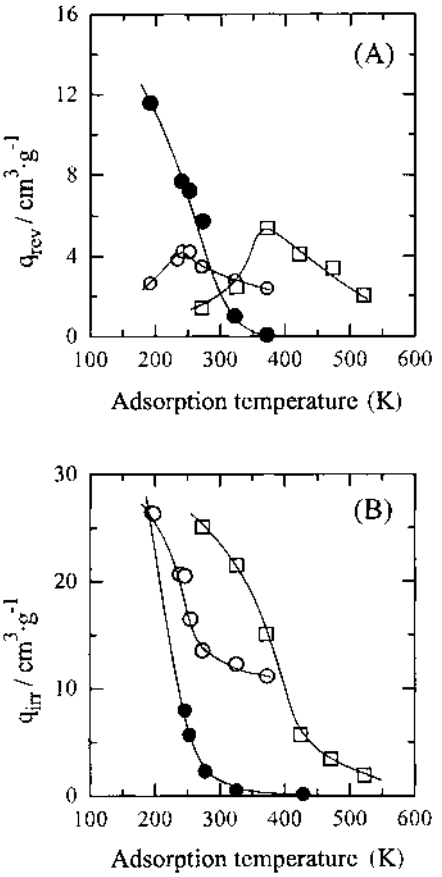

Fig. 2 Temperature dependence of (A) q_{rev} and (B) q_{irr} of Cu-MFI-157 (○), Co-MOR-65 (□), and Ag-MOR-112 (●). The concentration of NO is 1910 ppm. (Reprinted with permission from Ref. 21.)

In real exhaust gases, various gases coexist such as NO_2, O_2, CO_2, SO_2, CO, and H_2O. Therefore, it is important from a practical point of view to clarify their influence on adsorption properties. The effect of each gas on amount of NO adsorption was examined on Cu-MFI (19). The preadsorption of NO_2 on Cu-MFI-147 resulted in the enhancement of q_{rev} (from 4.35 cm^3 g^{-1} without preadsorbed NO_2 to 7.14 after the preadsorption of NO_2). At low temperature N_2O_3 is known to be in equilibrium with NO and NO_2. Irreversibly adsorbed NO_2 can act as new active sites for the reversible adsorption of NO. When O_2, CO_2, or SO_2 are preadsorbed, q_{rev} was only slightly reduced (4.26, 4.25, or 3.92 cm^3 g^{-1}, respectively). CO and H_2O poison the adsorption (1.39 or 0.22 cm^3 g^{-1}, respectively). On the other hand, q_{irr} is always decreased by the preadsorption of these gases, though the extent is dependent on the preadsorbed gas.

B. IR Study of NO Species on Metal Ion–Exchanged Zeolites

NO species adsorbed on metal ion–exchanged zeolites and its derivatives have been extensively investigated by several spectroscopic techniques such as infrared (IR) spectroscopy, Raman spectroscopy, ultraviolet photoelectron spectroscopy (UPS), electron

energy loss spectroscopy (EELS), and X-ray photoelectron spectroscopy (XPS) techniques. Among these techniques, IR is the most popular and widely used for assigning the state of NO species adsorbed on zeolites. A few IR results of the NO species formed on zeolites will be introduced here; the IR results of NO adsorbed on metals and metal oxides have been described in previous reviews (25,26).

IR bands associated with NO species on metal ion–exchanged zeolites are listed in Table 2 (20,27–42). NO species detected on metal ion–exchanged zeolites are mainly classified into three types: (a) mononitrosyl species with or without the electron transfer from and to metal ion in zeolites, (b) dinitrosyl species, $(NO)_2$, and (c) NO derivatives such as NO_2, N_2O, NO_3, and N_2O_3, which are produced by disproportionation and oxidation reactions of NO.

The NO molecule has three electron pairs occupying bonding orbitals and one unpaired electron in an antibonding orbital. Therefore, the bond order of NO is 2.5. In gas phase, the N-O stretching frequency is observed at 1876 cm^{-1} (43). This band shifts to higher and lower frequencies when the electron transfers occur from the π^* level of NO to the d orbital of the metal atom ($M^{\delta-}NO^{\delta+}$) and from an occupied d orbital of metal atom to the empty π^* antibonding orbital of NO ($M^{\delta+}$-$NO^{\delta-}$). As shown in Table 2, the stretching frequency of NO adsorbed on metal ion–exchanged zeolite spans a wide range, 1940–1780 cm^{-1}, depending mainly on the type of cation present in the zeolite.

Three isomers are reported for $(NO)_2$: *cis*- and *trans*-ON-M-NO and an antisymmetrical compound, NO-M-NO. *cis*-$(NO)_2$ is the most common form in dinitrosyl NO adsorbed on metal ion–exchanged zeolites. Generally, *cis*-$(NO)_2$ gives asymmetrical and symmetrical stretching vibrations. The angle between two NO molecules, ON-M-NO (2θ), is given by the following formula:

$$I_{asym} - I_{sym}^{-1} = \tan^2\theta \tag{1}$$

where I_{asym} and I_{sym} are the integrated intensity of asymmetrical and symmetrical stretching modes, respectively (44). Reported values are, for example, 103° for Cu-MFI, 94–96° for Rh-FAU(Y), 145° for Fe- FAU(Y), and 123–149° for Co-FER and Co-FAU(Y), which also display a dependence on the type of zeolite cation.

The bands observed at 2120–2140 cm^{-1} are discussed in several papers. In earlier studies, the band at 2133 cm^{-1} was assigned to NO_2^+ according to Chao and Lunsford (45). Several years ago, however, the assignment became open to question. Very recently, Hadjiivanov et al. (46) attributed this band, using the isotropic tracer method, to NO^+. A few bands in the 1100–1700 cm^{-1} region have been assigned to monodentate nitrito (47,48) and nitro (49) species. Hadjiivanov (26) has summarized the position of IR bands for surface NOx species on metals, metal oxides, and zeolites containing metal ions (Fig. 3). This diagram is very helpful for the initial assignment of IR bands.

Regarding NO adsorption, the largest number of studies have been devoted to copper-containing zeolite systems. Of these, Cu-MFI predominates because it is active for catalytic NO decomposition, as will be discussed later. Cobalt-containing systems have also been studied extensively. These results will be briefly introduced below; NO species formed on other metal ion-exchanged zeolites were summarized in an excellent review by Hadjiivanov (26).

1. NO on Cu-Exchanged Zeolites

Figure 4 shows the IR spectra obtained after NO adsorption on Cu-MFI-81 activated at 773 K (27). In order to assign each absorption band, isotopically substituted NO was used.

Table 2 Infrared Spectra Results of NO Adsorbed on Metal Ion–Exchanged Zeolites

Metal	Zeolite	Frequency (cm^{-1})	Adsorbed species	Note	Ref.
Cr	FAU(Y)	1900	$(NO)_2$[sym]	On Cr^{3+}	29
		1775	$(NO)_2$[asym]		
		1650, 1260	NO_2^-	Monodentate nitrito	
		1370	NO_3		
	FAU(X)	1895	$(NO)_2$[sym]	On Cr^{3+}	
		1770	$(NO)_2$[asym]		
Mn	MFI	1966	NO	On Mn^{3+} (O^-)	30
		1935	NO	On Mn^{2+} $(O^-)(NO_2)$	
		1894	NO	On Mn^{2+} (OH)	
		1516	NO_2	Monodentate nitrito	
		1630	NO_3		
		1591	NO_3	Monodentate	
		1567	NO_3	Bidentate	
Fe	MFI	1920	$(NO)_2$[sym]	On Fe^{2+}	31
		1880–1878	NO	On Fe^{2+}	
		1835	$(NO)_2$[asym]	On Fe^{2+}	
		1620	NO_3	Bidentate	
		1570	NO_3	Monodentate	
	FAU(Y)	1917	$(NO)_2$[sym]	On a highly accessible Fe^{2+}	32
		1870	NO	On a sterically hindered Fe^{2+}	
		1845	NO	On an intermediate accessible Fe^{2+}	
		1815	$(NO)_2$[asym]	On a highly accessible Fe^{2+}	
		1767	NO	On a highly accessible Fe^{2+}	
Co	MFI	2120	NO_2^+		20
		1940–1935	NO^+	On Co^{2+}	
		1894	$(NO)_2$[sym]	On Co^{2+}	
		1810	$(NO)_2$[asym]	On Co^{2+}	
	FER	1930	NO^+		33
		1890	$(NO)_2$[sym]	On Co^{2+}	
		1810	$(NO)_2$[asym]	On Co^{2+}	
		1630	NO_2	Nitro	
		1610	NO_2	Monodentate nitrito	
		1560–1540	NO_3		
	FAU(Y)	1930–1886	NO	(Unstable at RT)	33
		1910	$(NO)_2$[sym]	On Co^{2+}	
		1830	$(NO)_2$[asym]	On Co^{2+}	
		1800	NO	(Unstable at RT)	
	BEA	1935	NO	On Co^{n+}	34
		1898	$(NO)_2$[sym]	On Co^{n+}	
		1816	$(NO)_2$[asym]	On Co^{n+}	
		1540	NO_2	Monodentate nitrito	
		Below 1300	NO_2	Chelating nitrito	
Ni	FAU(Y)	1895	NO	On Ni^{2+}	35
Cu	MFI	2240–2230	N_2O		27, 28
		1905–1904	NO^+	On an accessible isolated Cu^{2+}	
		1895	NO	On Cu^{2+} carrying extralattice oxygen	
		1906–1895	NO	On Cu^{2+}	
		1827–1825	$(NO)_2^-$[sym]	On Cu^+	
		1815–1807	NO^-	On Cu^+	
		1734–1730	$(NO)_2^-$[asym]	On Cu^+	
		1630–1619	NO_2[asym]		
		1340–1300	NO_2[sym], NO_3		
	FAU(Y)	1951–1946	NO	On an accessible isolated Cu^{2+}	28
		1912–1907	NO	On Cu^{2+} carrying extralattice oxygen	

Table 2 (*continued*)

Metal	Zeolite	Frequency (cm^{-1})	Adsorbed species	Note	Ref.
		1902–1891	NO	On isolated Cu^{2+} moved to accessible position	
		1825	$(NO)_2$[sym]	On Cu^+	
		1732–1740	NO	On Cu^+	
		1796–1802	$(NO)_2$[asym]	On Cu^+	
		1400	NO_3		
Rh	FAU(Y)	1900	NO	On Rh^+	36
		1855	$(NO)_2$[sym]	On Rh^+	
		1780	$(NO)_2$[asym]	On Rh^+	
Pd	MFI	1881	NO	On Pd^{2+}	37
		1836–1833	NO	On Pd^{2+} (H_2O or NO_2)	
		1818	NO	Bent NO	
		1656, 1621, 1576	NO_2, NO_3		
	FAU(Y)	2175, 2025	NO	On Pd^{3+}	38
		1865	NO	On Pd^{2+} in supercage	
		1780—1795	NO	On Pd^{2+} in sodalite	
Ag	MFI	1630	NO_3	Bridging	39
		1576	NO_3	Bidentate	
		1440	NO_2	Monodentate nitrito	
	FAU(Y)	1884	NO	In $[Ag(I)NO]^+$	40
Au	MFI	1837	$(NO)_2$[sym]	On Au^+	41
		1817	NO	On Au^+	
		1741	$(NO)_2$[asym]	On Au^+	
		1620, 1302	NO_2	On Au^+	
	FAU(Y)	2240, 2200	N_2O		42
		1817	$(NO)_2$[sym]	On Au^+	
		1736	$(NO)_2$[asym]	On Au^+	
		1904, 1571, 1305	N_2O_3	On Au^+	
		1400	NO_3	On Au^+	

All bands observed in spectrum c in Fig. 4, measured in the presence of pure ^{15}NO, shifted to the respective lower wavenumbers according to theoretical calculation of the frequencies. Moreover, the presence of $(NO)_2$ could be demonstrated by the isotope tracer method (compare spectra b, c, and d).

The band assigned to Cu^--NO^+ (the δ sign has often been omitted in the literature) formed on Cu-MFI appears at 1906 cm^{-1}. This species is formed on isolated copper ions having a square-pyramidal configuration and have a linear configuration of Cu-N-O (50–52). The band at 1898–1895 cm^{-1} was also assigned to Cu-NO^+, but these copper ions have an adjacent O^- anion (53,54) in a square-planar configuration, although this band is not seen in Fig. 4. The band assigned to Cu^{2+}-NO^- was detected at 1813 cm^{-1} (27,48,55). Electron spin resonance (ESR) results with well-resolved Cu and N hyperfine structure revealed that the Cu^{2+}-NO^- species possesses an end-on bent structure (56–58) and quantum chemistry calculations supported the above geometries (59,60). When the pressure of NO increased, two IR bands associated to dinitrosyl species, Cu^{2+}-$(NO)_2$–, were observed at 1827 and 1734 cm^{-1} (27). IR results of Zecchina et al. (61) demonstrated the reversible interconversion between Cu^{2+}-NO^- and Cu^{2+}-$(NO)_2^-$ through the equilibrium Cu^{2+}-NO^- + NO = Cu^{2+}-$(NO)_2^-$.

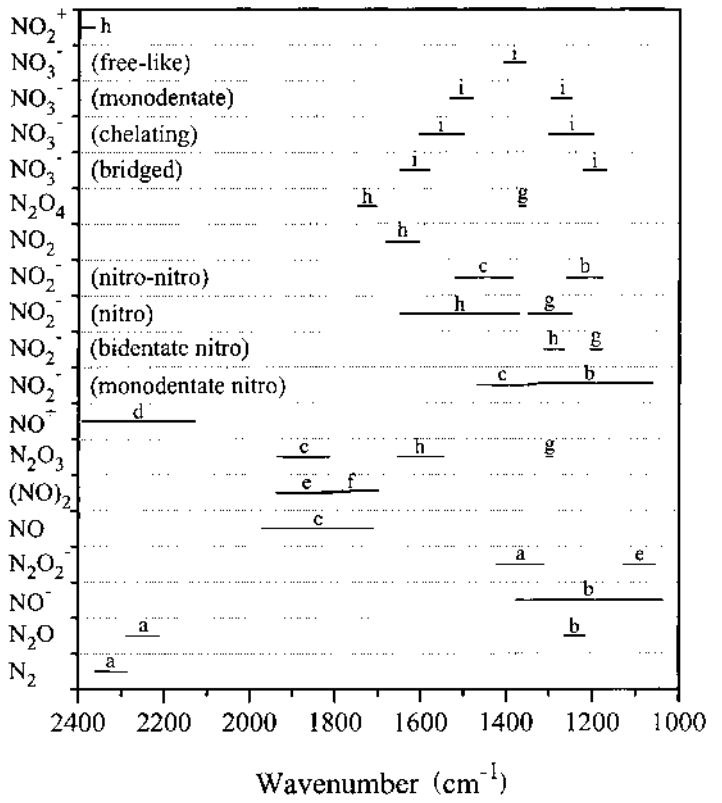

Fig. 3 N-N and N-O stretching modes of surface NxOy species. a, ν(N-N); b, ν(N-O); c, ν(N=O); d, ν(N≡O); e,ν_s(N-O)$_2$; f, ν_{as}(N-O)$_2$; g, ν_s(NO$_2$); h, ν_{as}(NO$_2$); i, ν(NO$_3$). (Reprinted with permission from Ref. 26.)

IR data have usually been discussed in connection with redox properties of copper zeolites. The reduction of Cu^{2+} ions to Cu^{+} ions upon prolonged evacuation at high temperature has been recognized in Cu-MFI (62) as well as Cu-FAU(Y) (63). As expected by the above IR results (27), the adsorption of NO on Cu^{2+} and Cu^{+} ions in zeolites gave Cu-NO^{+} and Cu^{2+}-NO^{-}[or Cu^{2+}-$(NO)_2^{-}$], respectively. Concerning the formation of surface NO species, it is interesting to know the distribution of Cu^{2+} and Cu^{+} ions in Cu-MFI evacuated at 773 K (62). The amounts of Cu^{2+} and Cu^{+} are shown in Fig. 5, which were estimated from ESR and CO adsorption measurements, respectively. Although the distribution was changed with copper loading, approximately 40% of Cu^{2+} ions in Cu-MFI with Cu/Al > 0.5 were readily reduced to Cu^{+}.

2. NO on Co-Exchanged Zeolites

When NO was adsorbed on Co-MFI, very intense bands appeared at 1847 and 1820 cm^{-1}, as shown in Fig. 6 (20). The former could be assigned to the symmetrical stretching mode of dinitrosyl species and the latter to the asymmetrical mode. Additional weak bands were also detected at 2120 and 1948 cm^{-1}, attributed to NO_2^{+}(or NO^{+}) and NO^{+}, respectively. The dinitrosyls are typical of cobalt ion–containing zeolite systems. The bands are usually observable in 1900–1890 cm^{-1} and 1816–1810 cm^{-1}. The band frequency of

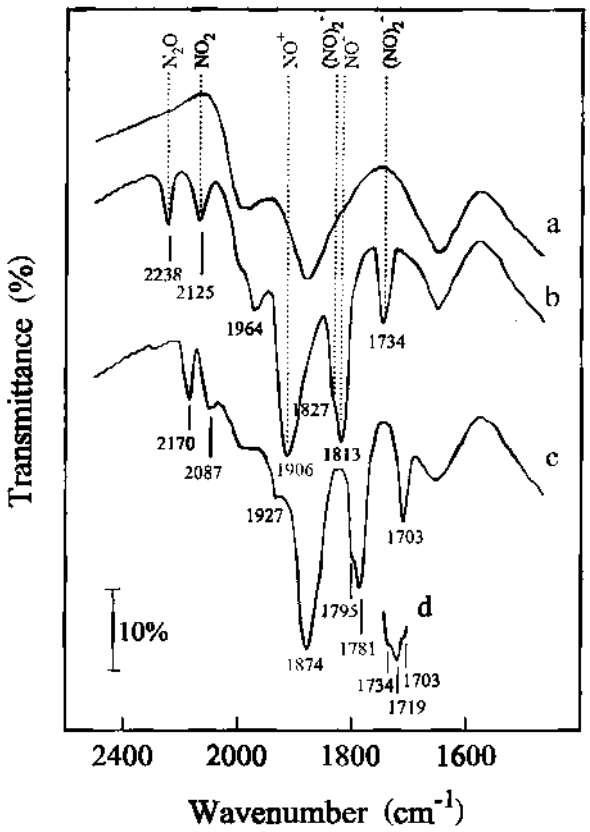

Fig. 4 IR spectra of NO species formed on Cu-MFI-81 activated at 773 K in vacuum: (a) background spectrum, (b) exposure to ^{14}NO (18.2 Torr), (c) exposure to ^{15}NO (18.5 Torr), (d) exposure to ^{14}NO (9.0 Torr) + ^{15}NO (9.0 Torr). (Reprinted with permission from Ref. 27.)

dinitrosyls is less dependent on the support, but the angle of ON-Co-NO depends on the support: 119° for FAU(Y) and BEA, 122° for MFI, and 129° for FER (33,34,64). The amount of dinitrosyl increased with the Co loading in Co-MFI (65).

The dinitrosyl formed on Co-MFI was more stable than that on Co/SiO_2; the dinitrosyls on Co/SiO_2 were removed by evacuation at room temperature, while on Co-MFI they were observable even after evacuation at 473 K, as shown in Fig. 6b (20,66). These results demonstrate that NO species irreversibly adsorbed on Co-MFI are mainly dinitrosyls. Zhang et al. (20) have pointed out that at least two kinds of dinitrosyls with the ON-Co-NO angles of 99° and 123° exist on Co-MFI, based on the results of IR and temperature-programmed desorption (TPD) techniques.

C. ESR Studies of NO Molecules on Metal Ion–Exchanged Zeolites

ESR and related techniques can provide supplementary information the about geometrical structure of NO adsorbed on metal ion–exchanged zeolites (67–70), though it should be noted that ESR measurements of NO were conducted at low temperature (< 80 K). The NO molecule in the ground state ($^2\Pi_{1/2}$) exhibits orbital degeneracy of the π^* orbitals. The degeneracy is removed by the interaction between the NO molecule and

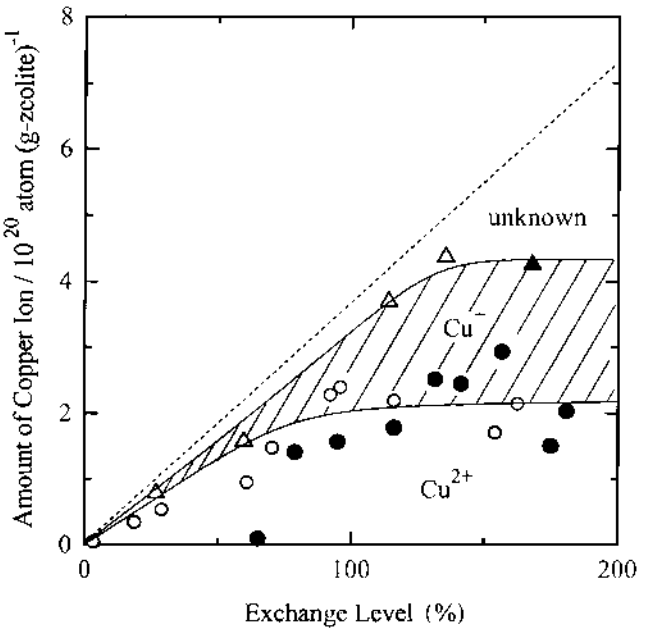

Fig. 5 Distribution of copper ions in Cu-MFI as a function of exchange level after oxygen treatment at 773 K. Amounts of Cu^{2+} (○, ●) and Cu^{+} (△, ▲) were estimated by ESR and CO adsorption measurements, respectively. The hatched region indicates the amounts of total copper ions in Cu-MFI. Open symbols: repeated ion exchange using aqueous copper(II) acetate solution. Closed symbols: ion exchange by addition of ammonia into aqueous copper(II) nitrate solution. (Reprinted with permission from Ref. 62.)

an electrostatic field, which is the case of, say, the molecule trapped by a cation in the zeolite lattice. Figure 7 shows one possible adduct with the Na cation and the valence orbitals of the NO molecule. Considering the energy-level diagram of the molecular orbitals of NO interacting with a metal ion (Fig. 7), an approximate relation between the orbital separation and the experimental values of the *g*-tensor components can be obtained (70).

$$\begin{aligned} g_{xx} &= g_e \\ g_{yy} &= g_e - 2(\lambda/\Delta) \\ g_{zz} &= g_e - 2(\lambda/\delta) \end{aligned} \tag{2}$$

Here Δ is the energy separation between the σ and π^* orbitals of NO, and δ is the separation between the π^* orbitals of NO, which are originally degenerate but split by the interaction with the metal ion.

Lunsford (67) first reported the ESR spectra of NO adsorbed on Na-FAU(Y) and NH_4-FAU(Y) zeolites. Gardner and Weinberger (68) observed similar spectra for NO adsorbed on Na-LTA, Ca-LTA, Na-FAU(X), and H-MOR. The spectra reported for these zeolites were very broad and ill resolved. Kasai and Bishop (69) noticed that the spectra for NO adsorbed on Ba-FAU(Y) and Zn-FAU(Y) zeolites become sharp after keeping the samples at room temperature for several days. In these earlier studies, however, ESR spectra were recorded mainly at 77 K. Yahiro et al. (71,72) have obtained

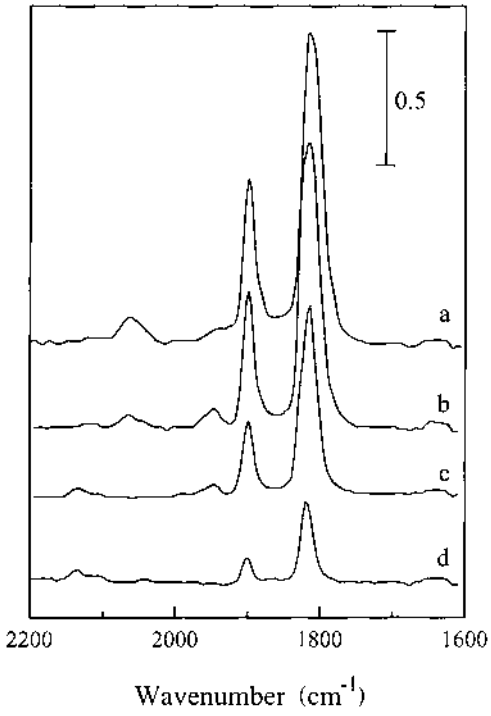

Fig. 6 IR spectra of NO adsorbed on Co-MFI-94 after (a) introduction of NO (54 torr), (b) evacuation at room temperature, (c) evacuation at 423 K, and (d) evacuation at 523 K. (Reprinted with permission from Ref. 20.)

sufficiently resolved ESR spectra by low-temperature measurements (< 77 K) and determined the exact ESR parameters. ESR spectra of NO adsorbed on Na-LTA, Na-MOR, and Na-MFI zeolites, which were recorded at 5.0 or 4.2 K, are illustrated in Fig. 8 as examples (72). All show the well-resolved three different g-tensor components and the resolved y-component hyperfine coupling with the ^{14}N nucleus ($I = 1$), which can be assigned to one NO molecule adsorbed on a Na cation in a bent configuration. In

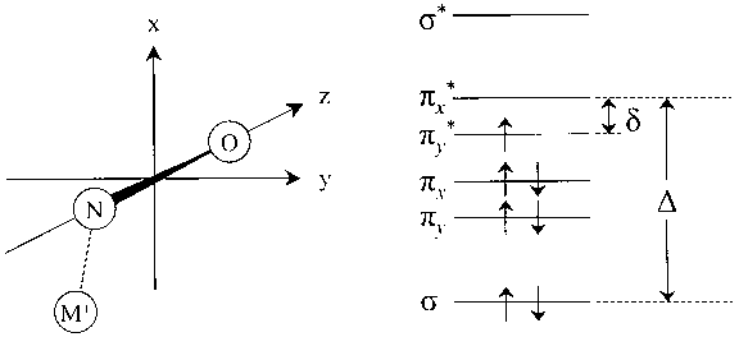

Fig. 7 The energy diagram (a) and the proposed structure (b) of NO adsorbed on a cation (M^+) in a zeolite matrix. (Reprinted with permission from Ref. 70.)

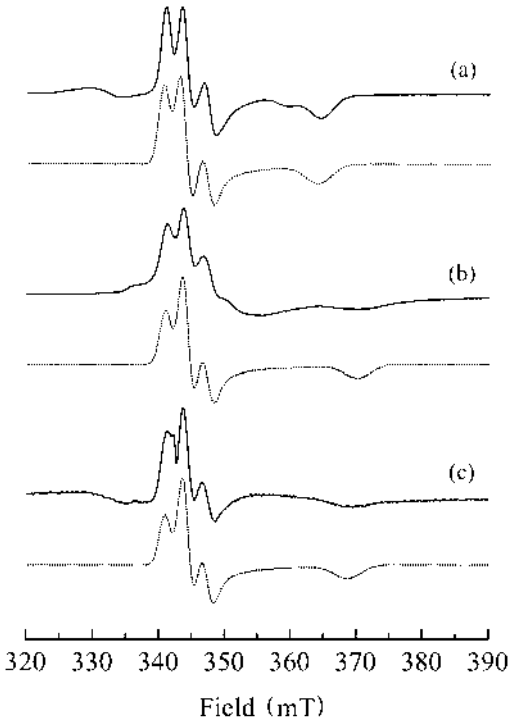

Fig. 8 Experimental (solid line) and simulated (dotted line) ESR spectra of NO (1.0 kPa) adsorbed on (a) Na-LTA (5.0 K), (b) Na-MOR (4.2 K), and (c) Na-MFI (4.2 K). The simulation was performed using Lorentzian lineshapes with anisotropic linewidths of 1.7, 1.7, and 4.0 mT for the x, y, and z components, respectively. The other parameters used are given in Table 3. (Reprinted with permission from Ref. 72.)

addition, Q-band ESR measurements reveal the presence of two types of NO adsorbates on Na-LTA at low and high temperature; one is attributed to a rigid form and the other to a rotational form (71).

ESR parameters of NO adsorbates on various zeolites are summarized in Table 3. The g_{zz} tensor component is very sensitive to the cation introduced into the zeolite, reflecting the degree of separation of the π* orbital. The ordering of Δg_{zz} ($= g_e - g_{zz}$) was $Na^+ > Ba^{2+} > Zn^{2+} \approx H^+$ for the FAU zeolite, $Na^+ > Zn^{2+}$ for the LTA zeolite, and $Na^+ > H^+$ for the MFI zeolite (73). It is clear that Na^+-exchanged zeolites showed larger Δg_{zz} than the divalent cation- or proton-exchanged zeolites, indicating the weaker electrostatic field associated with Na^+ ions. This result is consistent with earlier reports that the electrostatic field in the vicinity of divalent or trivalent cations and protons exchanged into the zeolites is stronger than that of monovalent cations (74). Δg_{zz} is also sensitive to the zeolite structure, Na-MOR > Na-MFI > Na-LTA, suggesting a stronger electrostatic field associated with Na^+ ions in LTA zeolite.

The hyperfine coupling to ^{27}Al nuclei ($I = 5/2$) was observed for proton-exchanged zeolites. Lunsford (67) observed broad spectra of NO adsorbed on H-FAU(Y) zeolites. This broad signal was assigned to NO adsorbates on trigonal aluminum at the oxygen-deficient sites of the framework. A similar spectrum was reported by Kasai et al. (70) on hydroxylated NH_4- FAU(Y) in which the aluminum hyperfine structure appeared. The

Table 3 g Tensors and Hyperfine Coupling (*hfc*) Tensors (^{14}N) Reported with NO Adsorbed on Various Zeolites

Zeolites	Temp. (K)	g-tensors			hfc (mT)			Ref.
		g_{xx}	g_{yy}	g_{zz}	A_{xx}	A_{yy}	A_{zz}	
Na-LTA	5.0	2.002	1.996	1.886	0	3.3	0	72
	110	1.979	1.989	1.909	0	3.0	0	72
	77	1.970	1.970	1.789				68
	77	1.980	1.987	1.905	~0	3.0	~0	77
Zn-LTA	77	1.999	1.999	1.918	~0	3.0	~0	77
Na-FAU(X)	77	1.970	1.970	1.79				68
H-FAU(Y)[a]	77	1.996	1.996	1.95				67
Na- FAU(Y)	77	1.989	1.989	1.86				67
	77	1.986	1.978	1.83	~0	2.9	~0	69
Ba- FAU(Y)	77	1.999	1.995	1.89	~0	3.4	~0	69
Zn- FAU(Y)	77	2.000	1.998	1.93	~0	3.0	~0	69
Na-MOR	4.2	1.997	1.995	1.855	0	3.2	0	72
	77	1.996	1.995	1.853	0	3.0	0	72
	77	1.990	1.990	1.859				68
Na-MFI	4.2	1.996	1.995	1.862	0	3.2	0	72
	77	1.994	1.992	1.862	0	3.0	0	72
	10	1.980	1.980	1.840	0	3.3	0	75
H-MFI[b]	78	1.997	1.997	1.950	1.6	1.6	0	75
H-MFI[c]	10	1.997	1.997	1.920	0	3.3	0	75

[a] hfc for ^{27}Al ($I = 5/2$) = 1.4 mT.
[b] hfc for ^{27}Al; A_{xx} = 1.6, A_{yy} = 1.6 mT, and A_{zz} = unresolved.
[c] hfc for ^{27}Al; A_{xx} = 0.9, A_{yy} = 0.9 mT, and A_{zz} = unresolved.

revelation of the aluminum hyperfine structure is considered to be due to the interaction of NO with the interstitial aluminum (hydro)oxy cations removed from the framework. Gutsze et al. (75) have also observed hyperfine coupling from ^{27}Al on H-MFI. They concluded that the NO molecule was bound to a "true" Lewis site in H-MFI. Such studies on the characterization of Lewis acid sites in zeolites have been vigorously carried out by Pöppl et al. using ESR and ENDOR techniques (76).

Kasai and Gaura (77) found that the ESR spectrum of NO in Na-LTA consisted of two signals, one due to the NO monomer and the other due to an unusual NO-NO triplet species. Yahiro et al. (71) have recorded Q-band ESR spectra of NO adsorbed on Na-LTA and proposed the precise parameters and the possible structure of NO-NO triplets. The facts that only the NO monomer was detectable when the NO pressure was low, while the triplet became dominant at higher NO pressure, and that the half-field signal due to the $\Delta M_s = 2$ transition was detected when the corresponding triplets were observed at the normal field of $g \approx 2$, secured the assignment of the NO-NO triplet species. The D parameter of zero-field splitting depends on the average distance between two radicals, R, according to the relation $D = 3g\beta/(2R^3)$. The values of R evaluated from the experimental D value ($331G$) were in the range 0.45 nm (71). This unusual NO-NO triplet was observed in the spectra of NO adsorbed on Li-LTA (78) and sulfated zirconia (79). However, ESR measurements provide less information about the exact location and/or the adsorption site of NO-NO triplets in Na-LTA zeolite. Very recently, a pulsed ESR measurement (80) was made that overcame this problem.

III. REMOVAL OF NO WITHOUT REDUCTANT-CATALYTIC DECOMPOSITION

A. Catalytic Activity

NO decomposition to molecular nitrogen and oxygen ($2NO = N_2 + O_2$) is the simplest, the most attractive, and the most challenging approach to NOx abatement. Several cation-exchanged zeolites have been applied as catalysts for NO decomposition. Iwamoto et al. first reported that Cu ions exchanged into the FAU (13) and MFI (15) matrix exhibit unique and stable activity among metal ions exchanged into zeolites (Table 1). In particular, the Cu-MFI having $Cu^{2+}/Al > 0.5$, of which details will be described in the following section, shows very high decomposition activity (81,82). This result was confirmed by Li and Hall (16). Since such a high catalytic performance of Cu-MFI is observed, it will be briefly introduced at the beginning of this section.

Figure 9A shows the temperature dependence of the decomposition reaction over Cu-MFI (81). No deterioration of the Cu-MFI was observed even after 30 h of continuous service. It should first be pointed out that there was incomplete conversion of NO to N_2 and O_2. The remaining nitrogen and oxygen balances were attributed to the formation of NO_2; Li et al. (83) indeed confirmed that the reaction of NO with the O_2 that is produced yields NO_2 both on the catalyst and in the homogeneous phase. Thus, it is clear that Cu-MFI has the ability to stoichiometrically decompose NO to N_2 and O_2, although a side reaction does occur. Second, maximal activity was observed around 823–873 K. Optimal temperature depends on the catalyst used and the partial pressure of NO in the feed (84). Several reasons have been proposed for the temperature dependence, but the most important factor is likely the desorption temperature of adsorbed/produced oxygen. Figure 10 shows TPD profiles of oxygen from several metal ion-FAU(Y) (85). It is clear that Cu-FAU(Y) desorbs large amounts of oxygen at temperature as low as 773 K, compared with the other metal ion–exchanged FAU(Y). The large desorption peaks of

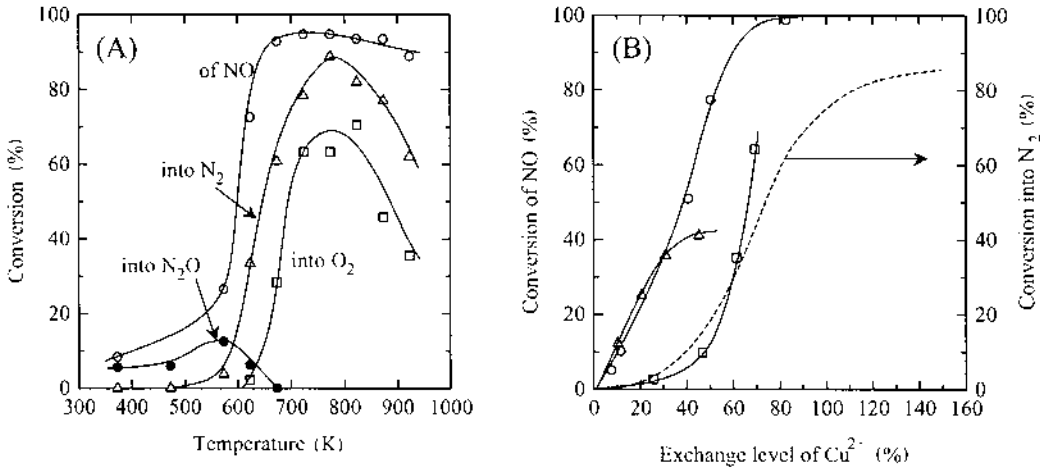

Fig. 9 Catalytic activity of Cu-MFI for decomposition of NO as a function of temperature (A) and catalytic activity of Cu-MFI (○), Cu-MOR (△), and Cu-FAU (□) as a function of the loading of copper ion (B). (A) Copper exchange level = 143%, NO = 1.0% and W/F = 4.0 g·s·cm^{-1}. (B) NO = 4.0 %, temperature = 823 or 873 K, and W/F = 4.0 g·s·cm^{-3} (solid line). NO = 1.0%, temperature = 723 K, and W/F = 4.0 g·s·cm^{-3} (dotted line). (Reprinted with permission from Ref. 81.)

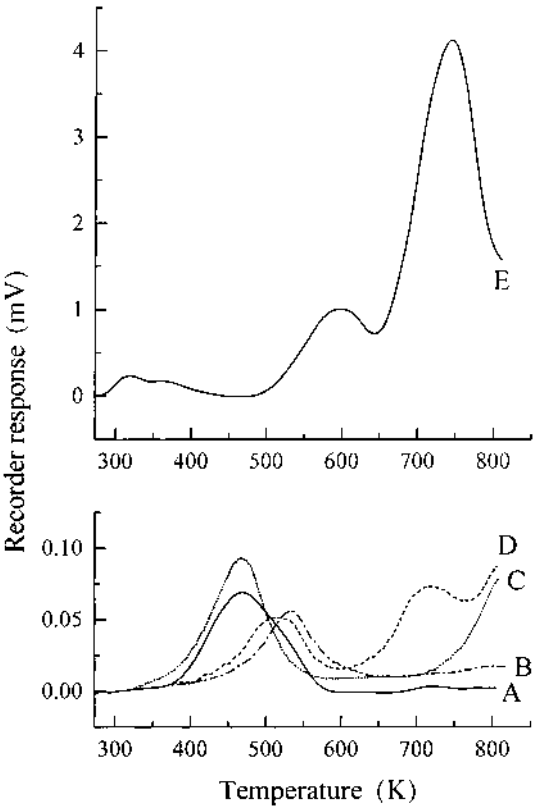

Fig. 10 TPD chromatograms of oxygen from several transition metal ion–exchanged FAU(Y) zeolites. A, Na-FAU(Y); B, Ni-FAU(Y); C, Mn-FAU(Y); D, Co-FAU(Y); and E, Cu-FAU(Y). (Reprinted with permission from Ref. 85.)

oxygen at low temperature were also observed for Cu-MFI (86). The desorption temperatures agree with the temperature at which the catalytic activities of Cu-zeolites starts. Recently, Ganemi et al. (87) pointed out that the temperature of maximal conversion coincides with the disappearance of surface nitrates, which are presumed to be site blockers for NO decomposition. The decrease in the catalytic activity at higher temperature was not attributable to the deactivation of the catalyst, since the activity did not change when the reaction temperature was raised and lowered stepwise between 773 K and 923 K (82). The change in the adsorption equilibrium of NO or in the properties of copper ions at elevated temperatures is a possible reason for the decreases, and further research is required.

The catalytic activities of copper zeolites for NO decomposition are strongly dependent on both zeolite structure and the degrees of Cu loading. Figure 9B displays these trends for various Cu-zeolite catalysts. Clearly Cu-MFI zeolite shows good catalytic activity. Note that the conversion to N_2 over Cu-MFI increased even in the region where the Cu/Al ratio is greater than 0.5 (the dotted line in Fig. 9B) (82). Many workers have reported similar results.

Although the discovery of exceptionally high activity of the Cu-MFI zeolite with $Cu^{2+}/Al > 0.5$ for NO decomposition is undoubtedly a milestone in the field of catalytic

deNOx technology, most of the experts believe that the activity of Cu-MFI is not yet sufficient in practice. Under real conditions, the catalyst should work in very low NO concentration, high oxygen concentration, and high space velocity. Because of this, modification of Cu-MFI or development of new catalytic systems has been studied in order to achieve higher performance in NO decomposition. In the case of zeolites or porous materials, various efforts have been reported. Wichterlová et al. (88) have found that Cu-MeAlPO-11s (Me = Mg or Zn) exhibited constant conversion in NO decomposition, and turnover frequency values at 770 K were comparable to those of Cu-MFI with high silica content. Schay et al. (89) found similarity in the catalytic activities of Cu-AITS-1 and Cu-MFI. Addition of a cocation such as Ni and Co (13), Ce (90), and Sm (47) to Cu-zeolites improves the activity for NO decomposition. It has been claimed that Co-MFI zeolite with Co in the framework has considerably higher activity for NO decomposition than Cu-MFI (91), although no data were reported for a continuous-flow system. In the case of metal oxides, Co_3O_4-based catalysts (92), $YBa_2Cu_3O_y$ (93), Sr^{2+}-substituted perovskite oxides (94), and Ba/MgO (95) have been reported as candidates for the catalyst. The NO decomposition activity of Pt metal has been established for a long time (96). Recently, the formation of a Tb-nitrate intermediate was observed to be important in NO decomposition over Tb-promoted Pt catalysts (97).

The relative catalytic activities of these catalysts are roughly compared in Fig. 11 (decomposition activity is plotted only roughly, since the experimental conditions vary with research group). The figure indicates that the key components for direct decomposition of NO are Cu and Co, and that their catalytic activities can be improved by addition of precious metal. It has been reported that an increase on the order of one order of magnitude in the turnover frequency could lead to a practical catalyst (98,99). NO decomposition still offers a very attractive approach to NOx removal. However, since any combustion process is going to produce 10–20% water vapor, one must focus on a catalyst that is stable for long times in such wet environments.

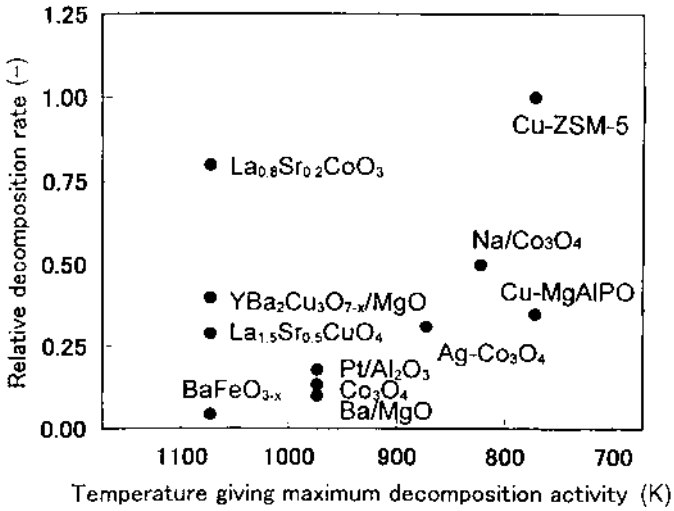

Fig. 11 Decomposition activity of various catalysts reported to date. (Reprinted with permission from Ref. 98.)

B. Characterization (and Activity) of Cu-MFI

1. Preparation of "Overexchanged" Cu-MFI

Cu-MFI samples having more than 0.5 Cu/Al are considered as nonstoichiometric compounds if the valence of the copper ion is considered to be +2. These samples display high catalytic activity in the NO decomposition reaction as described in the previous section. Such a catalyst is called "overexchanged" Cu-MFI. The overexchanged Cu-MFI is generally prepared by a repeated ion-exchange method using copper nitrate or acetate solutions; however, the mechanism of the overexchange reaction in zeolites has not been fully clarified. Schoonheydt et al. (100) first reported the overexchange of Cu-FAU(Y) in a solution of $CuCl_2$ and acetic acid. Iwamoto et al. (101) have proposed the following exchange schemes using MFI zeolite:

$$\begin{aligned} Cu^{2+}(s) + 2Na^{+}(z) + H_2O &\Longleftrightarrow Cu(OH)^{+}(z) + H^{+}(z) + 2Na^{+}(s) \\ Cu^{2+}(s) + H^{+}(z) + H_2O &\Longleftrightarrow Cu(OH)^{+}(z) + 2H^{+}(s) \end{aligned} \tag{3}$$

where s and z indicate "in solution" and "in zeolite", respectively. Vaylon and Hall (102) and Centi et al. (103) have independently suggested the formation of $Cu(OH)^{+}$ in MFI. One or more copper hydrates, such as $Cu_2(OH)^{3+}$, $Cu(OH)^{+}$, $Cu_2(OH)_2{}^{2+}$, and $Cu_3(OH)_2{}^{4+}$, in which the valence of copper is 2, may take part as the copper source (100,104); further spectroscopic studies on the geometrical structure of copper hydrates in the zeolite matrix are necessary.

Two easier methods than repeated ion exchange have been proposed to prepare the overexchanged Cu-MFI. The addition of basic compounds such as NH_4OH and $Mg(OH)_2$ into the initial copper solution during ion exchange resulted in excess copper ion loading in a single step (105). When ammonia was used as an additive, the exchange level of copper ion increased incrementally from pH 4 to 9, and above pH 9 all of the copper ions were loaded into MFI zeolite. On the other hand, the extent of conversion of NO increased with increase in pH, attaining a maximum at pH 7.5, and then slightly decreased at higher pH. The catalytic activity for NO decomposition of the overexchanged Cu-MFI prepared at pH 7.5 was comparable with that of overexchanged Cu-MFI prepared by the usual repeated ion-exchange method. An alternative method for preparing overexchanged Cu-MFI is solid-state ion exchange, which Karge and his coworkers (106) have discovered. When CuCl was mixed mechanically with H-MFI and heated at 573 K, overexchanged Cu-MFI could be prepared in a single step (107).

2. Reaction Mechanism of Catalytic NO Decomposition over Cu-MFI

Several excellent reviews (103,108–110) have been published regarding the reaction mechanism of NO decomposition over Cu-zeolites. It is apparent that no general consensus of opinion exists with respect to either the nature of the active site involved or the type of reaction mechanism occurring.

The main points of dispute can be summarized as follows:

1. Considerable evidence has been provided to indicate that Cu^{+} species participate in the reaction (27,54,111–113). On the other hand, the reaction of Cu^{2+} ion with no contribution of Cu^{+} has also been postulated (98). In our opinion, however, there is no doubt that the NO decomposition is a redox process.
2. The NO decomposition reaction is promoted on overexchanged Cu-MFI catalysts and this behavior may correlate with the availability of extralattice oxygen (ELO) species. The identity of the ELO is not clear. Iwamoto et al.

(27,112), Sachtler and coworkers (114,115), and Schmal et al. (116) have proposed that it is of the form Cu^{2+}-O^{2-}-Cu^{2+}, whereas Bell and coworkers (117) have suggested that the ELO is associated with isolated Cu^{2+} sites and is of the structure $Cu^{2+}O^{-}$ or $Cu^{2+}O^{2-}$. More recent investigations (110,118) have supported the presence of $Cu^{2+}O^{-}$ or $Cu^{2+}O^{2-}$ species.

3. The mechanism for coupling of nitrogen species to form N_2 is a topic of controversy. There are two problems to be solved. First, a significant problem is whether the number of copper ions working as the active site is one or two. The other has to do with the type of intermediate: nitrosyl, nitro, nitrate, and dissociatively chemisorbed NO species have all been suggested.

The first point of the third item will be discussed now in more detail. It was demonstrated that the most active catalysts are those with low Si/Al atomic ratios and with Cu exchange levels in the range of 90–150%. These results have led to two possibilities for copper active sites in Cu-MFI catalysts. One suggestion is that the active site responsible for the high catalytic activity is a unique dimeric Cu species that is stabilized by the zeolite framework (Fig. 12A). Adsorption of NO on this dimeric species to form a cuprous hyponitrite that decomposes to form N_2O and then N_2 is proposed to be a possible reaction mechanism (27,62,113–115,118–123). The species Cu^{2+}-O^{2-}-Cu^{2+}, Cu^{+}-O^{2-}-Cu^{2+}, and $Cu^{+}\ldots Cu^{2+}O^{-}$ are suggested (118,120,121) for this. Alternatively, a monomeric Cu site has been suggested as the active site by several researchers (61,107, 117,124,125) (Fig. 12B (103)). Giamello et al. (48) and Spoto et al. (61) have proposed that oxygen released in the transformation of dinitrosyl species remains bound to the surface and preferentially reacts with a NO molecule to form nitrite/nitrate species. Valyon and Hall (28,126) assume that a Cu^{+} dinitrosyl complex decomposes, via a hyponitrite intermediate, to Cu^{2+} ions, nitrous oxide, and extralattice oxygen ion. Although $Cu^{+}(NO)_2$ has been proposed as a precursor for N_2O formation in the studies, the lack of correlation between $Cu^{+}(NO)_2$ and N_2 formation (127) was reported and also first principles of quantum mechanical calculations (59) suggest that $Cu^{+}(NO)_2$ is not formed under reaction conditions. Thus, $Cu^{+}(NO)_2$ as a precursor would be ruled out. The $Cu^{2+}O^{-}$ or $Cu^{2+}O^{2-}$ species may form on the overexchanged Cu-MFI and act as the active sites (125).

Detailed characterization of Cu-zeolites has been carried out by Wichterlová and coworkers (51,128,129), Kuroda and coworkers (104,130,131), and other researchers (132,133) in the hopes of solving the above controversial reaction mechanism. For example, very recently the locations of Cu^{+} ions are proposed on the basis of experimental (129) and theoretical (132) studies, and their conclusions are in good agreement with each other. In addition, Kuroda et al. have claimed that zeolite having an appropriate Si/Al ratio, in which it is possible for the copper ions to exist as dimer species, may provide the key to the redox cycle of copper ion as well as catalysis in NO decomposition (131). This conclusion coincides with the results of theoretical calculation (133) in which bent Cu-O_x-Cu structures are found in Cu-MFI, and these are suggested to be the part of a catalytic cycle.

IV. REMOVAL OF NO WITH REDUCTANT

A. Continuous Reduction of NO, Oxygen, and Hydrocarbon Mixtures (HC-SCR)

1. Development of HC-SCR and Outline of Zeolite Catalytic Performance

Cu-MFI is the most active catalyst for the decomposition of NO. However, the activity greatly decreases in the presence of excess oxygen, water vapor, and SO_2, as mentioned

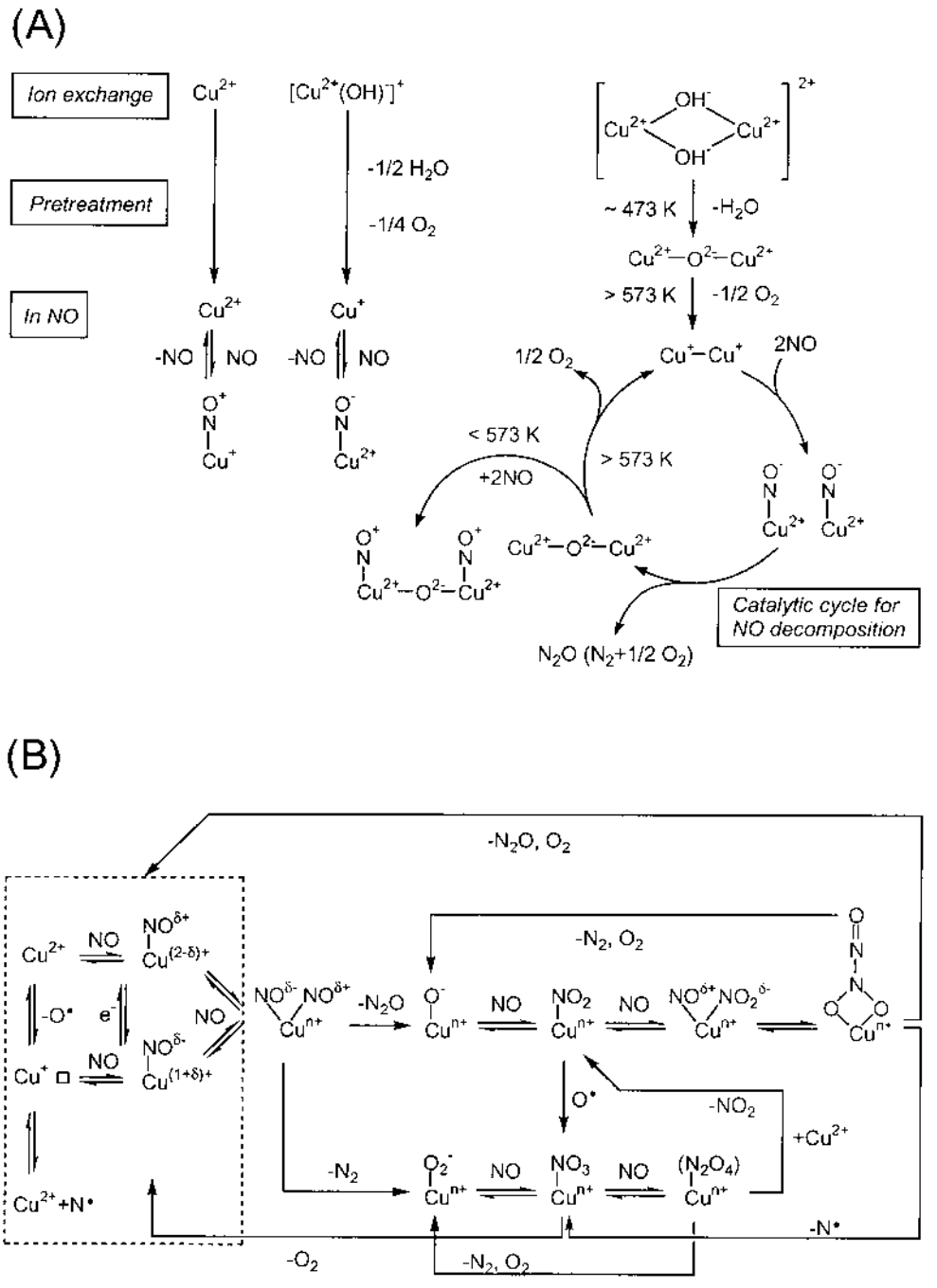

Fig. 12 Proposed mechanism for NO decomposition. Details are described in Sec. III.B.2.

in the previous section. The reduction of NO under such conditions can be accomplished by using hydrocarbons as reducing agents, which preferentially react with NO rather than oxygen. This process, selective catalytic reduction of NO with hydrocarbons in an oxidizing atmosphere (HC-SCR), was first reported over Cu-MFI in 1990 (17). The distinguishing characteristic of this new technology is that the presence of oxygen is indispensable for the progress of the reduction of NO. This new selective reduction of NO proceeds even in the presence of excess O_2 and has the possibility to overcome the disadvantages of the present reduction systems, NH_3-SCR, and the three-way catalytic system. Several reviews (14,134) have already summarized the progress of HC-SCR up to 1996.

Many catalysts have since been reported as active in HC-SCR. Some zeolite-based catalysts show high initial activities with either hydrocarbons or ammonia as reducing agents. A few examples are shown in Table 1 and Fig. 13. So far, however, the hydrothermal stability of zeolite catalysts appears to be limited. Hydrothermal deactivation can have several causes, such as structural collapse, dealumination, agglomeration of active cations to small oxide islands, and migration of the cations to inaccessible sites. As the stability is of major importance for applications, improvement of zeolite catalysts will have to include stability as well as initial activity. Alumina, some solid acids, and composite metal oxides have also been reported as active catalysts. In the case of metal oxide catalysts, the reaction rates are not sufficient, which means that a large reactor or low gas hourly space velocity is needed in practice.

As expected, all of the catalytic activities have been measured under the unique experimental conditions of the respective researchers. The hydrocarbons used, the con-

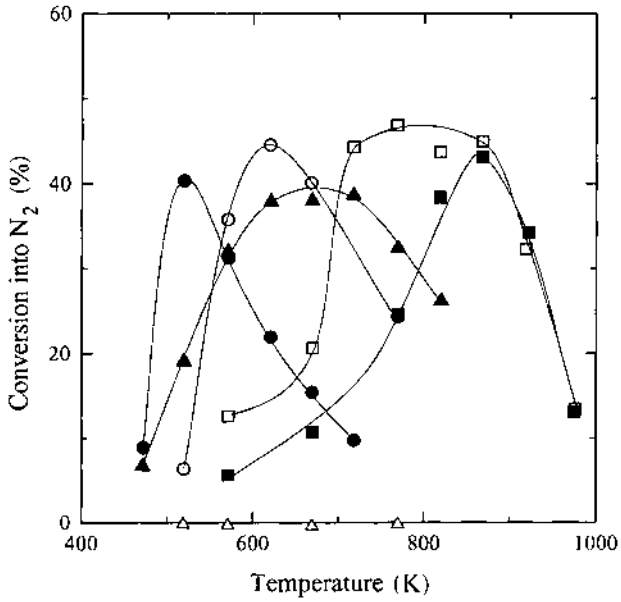

Fig. 13 Temperature dependence of catalytic activities of various cation-exchanged MFI zeolites. ○, Cu-MFI-102; ●, Co-MFI-90; ■, Zn-MFI-96; ▲, H-MFI-100; □, Ag-MFI-90; △, Na-MFI-100. Catalyst weight = 0.5 g, NO = 1000 ppm, C_2H_4 = 250 ppm, O_2 = 2%, total flow rate = 150 cm^3 min^{-1}. (Reprinted with permission from Ref. 14.)

centrations of the respective reactants, the space velocity, the shape of the reactor, and the pretreatment of the catalyst can all influence the reaction results and, therefore, the apparent catalytic activities. For example, we can employ ethene as reductant and probably obtain good results when we use a catalyst with high performance for hydrocarbon oxidation, while the use of propene could be recommended for the catalysts with low oxidation power. With the catalysts not so active for hydrocarbon oxidation, use of a low space velocity will promote high conversion of hydrocarbons and NOx. The molar ratio of NOx and hydrocarbons also affects the catalytic activity for deNOx reaction. With all this in mind, the many results reported are plotted in one figure to reveal general features of HC-SCR (14). In Fig. 14, differences in experimental conditions are not taken into account at all. Open circles, closed circles, and triangles correspond roughly to precious metals, microporous materials, and metal oxides, though there are many combined catalysts. The active temperature regions of catalysts clearly depend on the type of active centers. Precious metal catalysts are active at the lowest temperatures, transition metal ion–exchanged zeolites work at the middle-temperature region, and the active temperatures of metal oxide catalysts are the highest. Figure 14 also indicates that the active components are Pt, Cu, Co, Fe, Ag, In, Ga, Sn, and so on, and that the supports used are frequently zeolites and alumina. This author's assumption is that practical applications are more likely to be realized using precious metal–, Cu-, Co-, or Fe-containing catalysts. For lack of space, Cu and Fe will be reviewed here in more detail, and the reader is referred to the literature regarding investigations on Pt (135), Pd (136),

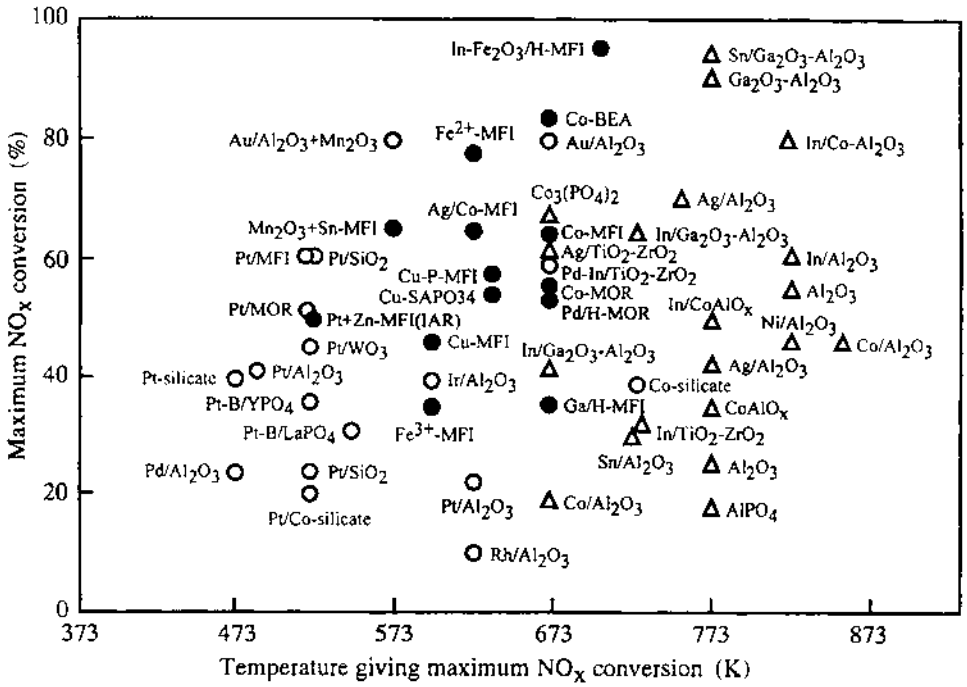

Fig. 14 Reduction activity of various catalysts reported to date. Open and closed circles and triangles roughly correspond to precious metals, microporous materials, and metal oxides. Changes in catalytic activity resulting from differences in experimental conditions have not been taken into account. (Reprinted with permission from Ref. 98.)

Rh (137), Ag (138), and Co (139); the catalytic performance of other metal-containing zeolites is covered in an excellent review (140).

When we consider practical application of the present HC-SCR method, probably the best way will be the simultaneous abatement of NOx and hydrocarbons on one catalyst bed in a continuous flow. The second best method would be the separation of oxidation of NO to NO_2 and reduction of NO_2 with hydrocarbons. These methods are discussed in the next two sections, respectively.

2. Copper Ion–Exchanged MFI Zeolites

The catalytic activity of Cu-MFI for the selective reduction of NO with C_2H_4 is shown in Fig. 15A as a function of reaction temperature (141). The temperature at which conversion to N_2 reaches its maximal value corresponds to the temperature at which hydrocarbon oxidation is complete. At higher temperatures, conversion to N_2 decreases probably due to the more rapid oxidation of hydrocarbon with oxygen. It should be noted that the active temperature region of HC-SCR is lower than that of NO decomposition. The catalytic activities for HC-SCR have been compared for samples prepared by different methods: mechanical mixture and ion exchange (142). Cu-MFI prepared from the mechanical mixture of H-MFI and $CuCl_2$, followed by heating at 673 K, gives comparable activity at 600–800 K to a sample prepared by a conventional ion-exchange method.

Figure 15B shows the maximal catalytic activity of three catalysts—Cu-MFI, Cu-MOR, and Cu-FAU(Y)—as a function of copper loading (143). On Cu-MFI and Cu-MOR catalysts, catalytic activities increase with Cu-exchange levels up to maxima at 80–100%, respectively, and then gradually decrease. This means that when too much copper is incorporated into zeolite, the efficiency of the catalyst tends to drop. This is probably because the oxidation activity for hydrocarbons is too high. This dependency is in contrast with the activity of Cu-MFI for NO decomposition, which increased even above the 100%

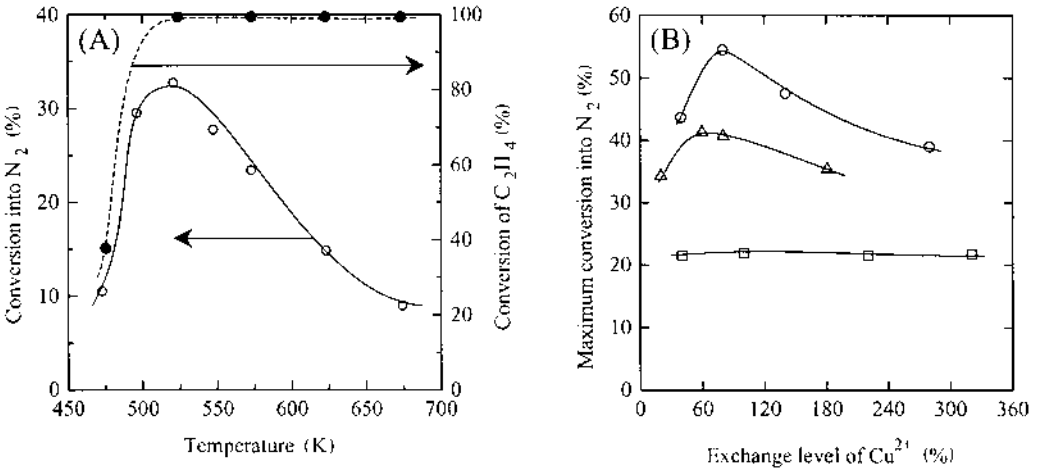

Fig. 15 (A)Temperature dependence of catalytic activity of Cu-MFI for selective catalytic reduction of NO with C_2H_4. Copper exchange level = 137%, NO = 1000 ppm, C_2H_4 = 250 ppm, O_2 = 2%, and W/F = 0.2 g·s·cm^{-1}. (B) Catalytic activity of Cu-MFI (○), Cu-MOR (△), and Cu-FAU (□) for selective catalytic reduction of NO. NO = 880 ppm, C_3H_6 = 800 ppm, O_2 = 4%, W/F = 0.12 g·s·cm^{-3}. (Reprinted with permission from Ref. 141.)

exchange level. On the other hand, the catalytic activity of Cu-FAU(Y) was almost constant independent of the degree of copper loading. Cu-BEA zeolite was also reported to show excellent activity (144,145). The activity of Cu-MFI increases with increasing SiO_2/Al_2O_3 ratio when the catalysts have similar copper loading (146).

Many hydrocarbons have been examined as reductants. On Cu-zeolites, most of the hydrocarbons tested were more or less active, although methane was not effective for the SCR reaction. Later, Co- (147), Ga- (148), In- (148), and Pd-zeolites (149) were proposed to be potential candidates for the catalyst in the CH_4-SCR reaction. The efficiency of NO removal is also dependent on the gas composition and the gas hourly space velocity (GHSV) (109). The hydrocarbons in diesel exhausts are better reductants than the trial mixtures used in laboratories, which is probably due to a higher concentration of hydrocarbon radicals in real exhausts (150). It is noteworthy that HC-SCR over Cu-MFI was not significantly inhibited by SO_2 (151), which is favorable for practical application.

Despite all of these positive results, Cu-zeolites in various catalytic reactions, including NO reduction, have two critical problems. One is that they are very sensitive to poisoning with H_2O. There are two kinds of suppression/deactivation: (a) fully reversible suppression by short exposure of the catalyst to water vapor, and (b) irreversible deactivation after the long-term service of the catalyst at high temperature in water vapor. When Cu-MFI was applied to actual diesel engine exhaust for a short time, it gave high N_2 conversions (150). Cu-SAPO-34 (152) and Cu-IM5 (153) catalysts showed higher durability in water than Cu-MFI. Deactivation correlates with the low thermal stability of zeolite lattice; treating the Cu-MFI catalyst at or above 823 K results in a deactivation even under dry conditions (154).

The mechanism for gradual deactivation under relatively mild conditions has not been identified. Formation of CuO particles (154) or clusters (155,156) and migration of Cu^{2+} ion into inert sites (157,158) have been suggested as the causes. Fresh Cu-MFI samples pretreated at 673–773 K usually show two types of ESR signals with $g_{//} = 2.31$–2.33 and $A_{//} = 140$–155 G (Cu_A), and $g_{//} = 2.27$–2.29 and $A_{//} = 155$–175 G (Cu_B). The spectra have been assigned to the Cu^{2+} species in square-pyramidal and square-planar coordinations, respectively. A few research groups (157–159) have independently reported that the treatment of Cu-MFI at 1073 K causes the elimination of the Cu_A and Cu_B species, the formation of new Cu_C species with $g_{//} = 2.30$–2.32 and $A_{//} = 155$–160 G, and the simultaneous dealumination of the zeolite lattice. It has been suggested that dealumination brings about the change in location of Cu ions and the resulting migration of Cu ions to inert sites is the origin of the deactivation under the mild conditions (158,159). On the other hand, Tabata et al. (155) have not found any evidence for dealumination under similar conditions but did observe the formation of Cu---Cu bonds by EXAFS. Therefore, the formation of CuO clusters is suggested for the deactivation. There is another report (156) in which $CuAl_2O_4$ formation is associated with the deactivation. Iwamoto et al. (160) have independently compared ESR, IR, X-ray diffraction (XRD), and ^{27}Al magic angle spinning NMR (MASNMR) spectra and the surface areas of the hydrothermally treated Cu-MFI with those of a fresh sample. The results indicate that the migration of Cu ions to inert sites without dealumination causes deactivation and that zeolite lattice changes occur under more severe reaction conditions.

There are many reports for improvement of the stability of Cu-MFI. Cu-containing silicate has been reported to show better stability than Cu-MFI (161). The coloading of La or Ce (90,162), Cr (163), or P (164) has stabilized the catalytic activity of Cu-MFI. In particular, the addition of P was very effective. A Cu-P-MFI catalyst

treated at 923 K for 50 h in water vapor possesses reduction activity at higher temperatures. The addition of Ca onto the Cu-P zeolite was reported to be effective for the further improvement of durability.

At present, two types of reaction mechanisms have been suggested for the role of hydrocarbons. Some research groups have proposed that no direct interaction between hydrocarbons and NO is required (161,165). In this mechanism, decomposition of NO proceeds first to yield N_2 and surface oxygen species, and then the hydrocarbons clean up the surface oxygen adsorbates. Alternatively, the hydrocarbon-O_2 mixture reduces the active sites for NO decomposition reaction, which occurs by a redox mechanism. Other researchers have claimed the direct interaction between hydrocarbons and NO (or NO_x) on the catalysts (33,49,166,167). In this view, carbonaceous deposits, partially oxidized hydrocarbons, hydrocarbons themselves, or ammonia are postulated as the active species, and NO, NO_2, N_2O_3, and NO_3^- are proposed as the reactive nitrogen oxides. The latter mechanism is promising on Cu-MFI.

Many types of reaction mechanisms have been suggested on Cu-zeolites, the majority of which are still controversial. It is important for this research to note whether the data are obtained on overexchanged or on low-exchanged Cu-MFI (166). For example, some types of adsorbed NO are observed on overexchanged ones, while nitrosyl and nitrite-nitrate adsorbates were found on low-exchanged ones. The behavior of some surface N–containing intermediates such as nitrosopropane (168) is highly dependent on the exchange level of copper and the state of the catalysts. The role of N-containing surface species in HC-SCR has been summarized recently by Sachtler and coworkers (169).

3. Iron Ion–Exchanged MFI Zeolites

Numerous zeolite-based catalysts show promising activities for the reduction of nitrogen oxides with hydrocarbons but have not yet been commercialized for this purpose, except for Co-BEA zeolite. This is due to a lack of long-term stability, especially in the presence of sulfur dioxide and water vapor. Recent results indicate that iron ion–exchanged MFI zeolites exhibit remarkable stability under realistic off-gas conditions. Feng and Hall (170,171) reported a very high and stable catalytic activity for the reduction of NO with *iso*butane at 723 K in the presence of 20% H_2O and 150 ppm SO_2. Although the very high catalytic activities could not be reproduced by other groups (172–174) or by themselves (175), Chen and Sachtler clearly demonstrated that the high activity under wet conditions continues for at least 100 h at 623 K (173) and that activities decrease in the order Fe-BEA > Fe-MFI > > Fe-FER > Fe-MOR ≈ Fe-FAU(Y) (176). The problem concerning reproducibility of active catalysts is attributed to the difficulty of zeolite preparation containing unstable Fe^{2+} ions, per the following discussion.

Active Fe-MFI catalysts described thus far have been obtained under anaerobic conditions. This is because Fe^{2+} ions are easily oxidized in aqueous medium giving rise to iron hydroxide species (177). In the first report, iron oxalate was used in a glass apparatus with separate supplies of zeolite and iron salt under nitrogen atmosphere until the Fe/Al atomic ratio reached 1.0. However, Chen and Sachtler (172) could not achieve such a high degree of ion exchange in their attempt to reproduce the results. A better way to introduce iron was found to be the sublimation of a volatile iron salt, $FeCl_3$, into the hydrogen form of the parent zeolite under inert atmosphere (172,173). Pophal et al. (178) employed iron sulfate during aqueous ion exchange at 323 K under N_2. On the other hand, Kögel et al. have used the solid-state ion-exchange procedure (106,179,180) to prepare iron-exchanged MFI zeolites in air (174,181). This method, using $FeCl_2$ $4H_2O$ in air, would be useful for the preparation of practical Fe-zeolites catalysts.

The activity of Fe-MFI can be improved by the addition of La (173). In particular, the activity at higher temperatures is vastly increased and the temperature window of Fe-MFI is wider. Recently, 10-h exposure of Fe-MFI, prepared by sublimation of iron chloride, to wet exhaust gas at 873 K was reported to cause severe deactivation of the catalyst (182). This temperature is too high for maintaining the zeolite structure. It was suggested that the second sublimation brings about an improvement in the stability of the Fe-MFI catalyst, though its deNOx activity decreases. The state of Fe dispersion in Fe-MFI was investigated by means of IR, TPD, and TPR. For samples with an Fe/Al ratio less than 0.56, Fe exchanges with Brønsted acid protons on a 1:1 basis, while higher weight loadings of Fe result in the formation of small particles of FeO_x (183) or dispersed Fe oxide clusters (184). For $Fe/Al < 0.19$, most of the Fe is present as Fe^{3+}, and at higher values of Fe/Al there is a mixture of Fe^{3+} and Fe^{2+}. Meanwhile, it was clarified that the population of oxo complexes that lose oxygen by heating depends on the Si/Al ratio. This dependence is in qualitative agreement with the model of (2+)-charged binuclear ions $[HO\text{-}Fe\text{-}O\text{-}Fe\text{-}OH]^{2+}$. Upon reacting with NO, the bridging O atom would yield NO_2 (176,185). Recently, Prins et al. (186) reported the presence of diferric (hydr)oxo-bridged binuclear clusters in Fe-MFI ($Fe/Al = 1$), whose structures differ from those reported previously. This complex was located at the ion-exchange positions of the zeolite. The reported binuclear ions (or clusters) would be a key compound in HC-SCR.

The study on reaction mechanism on Fe-MFI has recently been started by several groups (31,169,187). All researchers suggest the formation of nitrogen-containing adsorbates on the catalyst and the subsequent reaction with gas phase NO or NO_2. Recent Fourier transform infrared (FTIR) analysis of the gaseous products on Fe-MFI showed substantial production of HCN (188), which was strongly dependent on the dry/wet conditions. These results may be helpful in elucidating the reaction mechanism.

An interesting feature of Fe-MFI is that not only NO but also N_2O can be reduced to nitrogen using hydrocarbons. Concern about nitrous oxide emissions has recently increased due to the reported potential for global warming and stratospheric ozone depletion (189). Segawa and coworkers (178) used propene as a reductant and achieved high nitrous oxide conversion, also in the presence of oxygen and up to 15% water. Subsequently, it has been shown that substantial conversions of NO and N_2O can be achieved simultaneously, using propane as reducing agent (174,181).

B. Two-Stage Treatments: Oxidation of NO to NO_2 and Subsequent Reduction of NO_2 with Hydrocarbons

Various metal oxides, precious metals, and metal ion–exchanged zeolites have been reported to be active for HC-SCR, and there have been many discussions concerning the reaction mechanism. Much attention has been given to the concept that NO is first oxidized to NO_2 with oxygen, and then the resulting NO_2 reacts with hydrocarbons to form an active intermediate for the formation of N_2. Other efforts have been devoted to developing bifunctional catalysts with an oxidation and a reduction site. For example, in the reaction systems of $NO + O_2 + CH_4$ on Pt/In/MFI (190) and of $NO + O_2 + C_3H_6$ on the physical mixture of Mn_2O_3 and Ce-MFI (191), platinum and Mn_2O_3 are reported to be active for the oxidation of NO to NO_2, respectively, and the other components are suggested to be the sites for reaction of resulting NO_2 with hydrocarbons. One of the most significant problems for these systems is that the oxidation catalyst or site for NO is often active for oxidation of the hydrocarbons, which would result in decreased efficiency of the

reductant. In the case of methane reductant, Pt can be used for the NO oxidation because of the low oxidation activity of Pt to CH_4 (190). For propane, Mn_2O_3 or CeO_2 should be employed because Pt and other oxide catalysts are too active for this hydrocarbon's oxidation (191).

An alternative approach for solving this problem consists of separating the oxidation and reduction processes. Two suggestions are time-resolved HC-SCR and site-resolved HC-SCR. The former is an NOx storage-reduction (NSR) system developed by Toyota Motor Co. and used in practice for lean-burn gasoline engines (192). The latter concerns the intermediate addition of reductant (IAR) system suggested by the present author's group (193).

1. NOx Storage-Reduction

A NOx storage catalyst is used in an engine that operates alternatively under lean or rich conditions (192,194). During lean operation, the nitrogen oxides in the exhaust are stored in the catalyst. Upon turning the engine to rich conditions for a short period, the stored NOx is released and reduced with hydrocarbons and CO over the catalysts. The NOx storage catalyst reported by Takahashi et al. (192) consists of noble metals (mainly Pt), alkaline earth metals (mainly Ba), and alumina. Noble metals catalyze oxidation and reduction reactions of NOx, alkaline earth metals are NOx storage components, and alumina is a high surface area support. The concept of NSR reaction is summarized in Fig. 16.

Several metal oxides, mainly alkaline earth metal oxides, are effective in forming nitrates with NO_2, which decompose at high temperatures (194). The metal oxides can be used for reversible storage of NOx. Typical examples of such metals are barium and strontium. The reaction sequence in the NOx storage/release cycle has been discussed (195). Before an NOx storage reaction, the oxidation of NO to NO_2 is assumed to be a necessary initial step during lean conditions. With BaO as the storage component, the storage would proceed through the following reaction:

$$2NO_2 + O + BaO \Rightarrow Ba(NO_3)_2 \tag{4}$$

However, this simple step already includes several uncertainties. The atomic oxygen in the left side of reaction is needed for mass balance but has not been proven experimentally. The types of barium compounds are also uncertain. The decomposition of stored NOx during the rich period would be reverse of the above reaction. Several areas of confusions are as follows. Takahashi et al. reported that the amount of NOx stored increases with increasing oxygen content in the exhaust gas (192). In contrast, it has been reported that the capacity increases when the oxygen content increases from 0% to 3%, but above 3% no effect was exhibited (196). Bögner et al. (197) concluded that their catalyst stores NOx as a surface metal nitrate. Stable carbonates are formed on BaO whereas no carbonate is formed on barium aluminate, and the structure of the nitrates formed on these two compounds is very different (198). An N-bounded nitrate is formed on barium aluminate and not on bulk BaO.

Some problems still remain, mainly concerning deactivation of the catalysts. Deactivation is due to reaction of the adsorbents with gas phase compounds and to particle growth of both the precious metals and the adsorbents (199). In particular, because of the formation of very stable sulfates, the resistance to sulfur poisoning of adsorbents must be improved (200). SO_2 was found to be accumulated in the catalysts as sulfate (201).

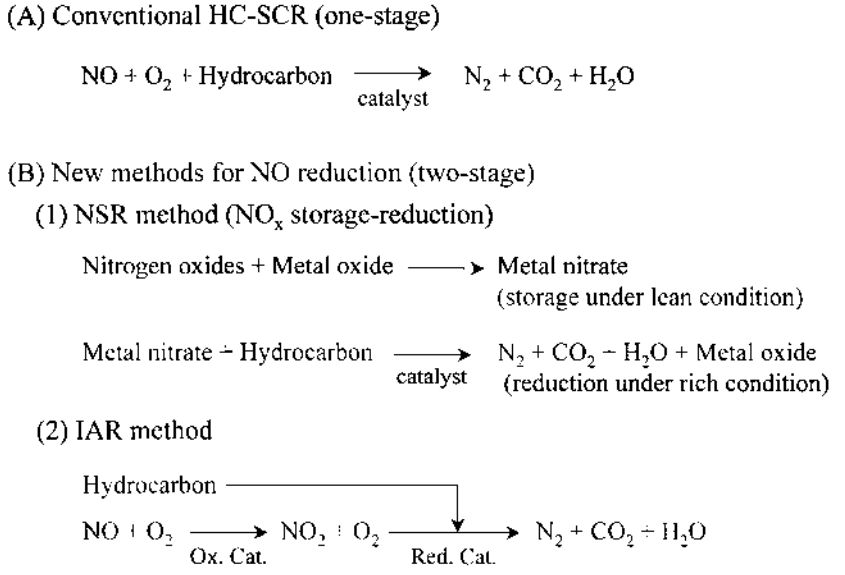

Fig. 16 Concepts of NSR and IAR methods (see Sec. IV.B). (Reprinted with permission from Ref. 98.)

2. Intermediate Addition of Reductant Between Oxidation and Reduction Catalysis

It is well known that diesel exhausts contain very small amounts of unburned hydrocarbons and that the concentration of NO is rather high (202). The addition of fuels or hydrocarbons into the diesel exhausts is required to reduce NO through the HC-SCR method. On the basis of the reaction mechanism of HC-SCR and the necessity of hydrocarbon addition, we have proposed a novel strategy to reduce NO selectively. This is intermediate addition of a reductant into the NO-containing exhaust between an oxidation catalyst of NO to NO_2 and a reduction catalyst to N_2 (IAR method) (193). The concept of the IAR method is also described in Fig. 16. The IAR method is expected to prevent the combustion or inefficient use of hydrocarbons with O_2 on oxidation sites. IAR experimental results may also be helpful in revealing the reaction mechanism of HC-SCR.

Pt-MFI has been used as the oxidation catalyst on the basis of previous results (203). Many kinds of metal ion–exchanged MFI zeolites have been examined as the reduction catalysts to investigate the validity of the IAR method. When H, Zn, Ag, In, Ga, Mg, Ba, Ca, and Na-MFI were used as the latter catalysts, the conversion levels of NO to N_2 greatly increased from those on the respective systems without the oxidation catalyst. On the other hand, conversions on Co, Cu, Mn, Ni, Fe, and Pt-MFI changed little with or without the preoxidation of NO. The combination of Pt-MFI and Zn-MFI has been found to be the most effective for the IAR method under the present conditions (193). For example, the degree of conversion of NO to N_2 at 573 K increased to 54% using the Pt- and Zn-MFI combination, from 5% on Zn-MFI alone or 6% on Pt-MFI alone. The efficiency of ethene (E_{HC}), namely, the molar ratio of the amount of NO reduced to that of ethene consumed, reached about 2, which is significantly higher than the 1.4 reached using conventional reduction on Cu-MFI.

These results show the potential effectiveness of the IAR method to reduce NO selectively with hydrocarbons in the presence of excess oxygen. Although the effect of water addition and the IAR reaction dependence on the partial pressures of the reactants remain to be clarified, it is clear that, if this method is employed, one does not need to develop a catalyst that oxidizes NO to NO_2 but rather one that does not oxidize the reductant. There are many possibilities for the proper combination of oxidation and reduction catalysts, depending on the conditions of exhausts and the kinds of reductants. In addition, the results would be useful toward understanding the HC-SCR reaction mechanism on each catalyst.

V. MOLECULAR DIFFUSION OF NOx IN ZEOLITES

Studies on not only the removal of NO_x but also on various catalytic reactions using zeolites have led to several critical unanswered questions, such as why zeolite-supported catalysts are more active than metal- and metal- oxide–supported catalysts, and which zeolite structure is the best and for what reasons. For example, the MFI structure is the most efficient support for the direct decomposition of NO, but the explanation is still obscure despite several plausible attempts (204). A large part in solving these questions would be to resolve the diffusion of reactants (or products) in zeolite channels and the interaction between the host zeolite (or the catalytically active site) and the guest molecule in the channel and/or cavity of zeolites. These issues will now be discussed briefly.

Zeolite catalysts have advantages over metal and metal oxide catalysts, such as providing coordinately unsaturated metal ions, enrichment of reactants in the open zeolite network, coexistence of metal cations and acidic protons, etc. On the other hand, a significant disadvantage for catalytic performance may be the high resistance of mass transfer in zeolite channels, i.e., sever intracrystalline diffusion. Tabata et al. (205) have found a dependence of HC-SCR activity on the primary crystal size of Co-MFI; the reaction rate on Co-MFI with large crystal size (1.3 μm, mean crystal diameter) was less than that with a small size (0.1 μm). A similar result was observed on Co-MOR (206). These results indicate that the rate of HC-SCR reaction on Co-zeolites is controlled by intracrystalline diffusion. In addition, the presence of SO_2 inhibited the diffusion of reactants with Co-BEA because the micropores in BEA are clogged or narrowed by the adsorbed SO_2 (34). Shichi et al. (207) have found that the type of reductant influenced the intracrystalline diffusivity in HC-SCR over Cu-MFI catalysts; the reaction rate of NO conversion was dependent on the crystal size in the $NO\text{-}C_2H_4\text{-}O_2$ reaction, but not in the $NO\text{-}C_3H_8\text{-}O_2$ reaction. This is caused by the stronger interaction of C_2H_4 with copper ions than that of C_3H_8, i.e., the adsorption properties of hydrocarbon on Cu-MFI play an important role in determining intracrystalline diffusivity.

Spectroscopic investigations of the physical and chemical properties of the intracrystalline void systems of zeolites have been carried out. One example utilizes ^{129}Xe NMR (204), which is a convenient, sensitive, and widely used tool for zeolite studies. Ito and Fraissard (208) first clarified the relation of the chemical shift, δ, to void space in zeolites by treating δ as the sum of terms of collisions between ^{129}Xe atoms and cage walls of zeolite, the exchangeable cations, or other ^{129}Xe atoms. Since then, there have been many applications to the study of void space in zeolites (209). Another example is ESR using nitrogen dioxide, NO_2, as a probe molecule at the gas–solid interface. The molecular dynamics of NO_2 adsorbed on Na-FAU(X) zeolites has been analyzed by the

temperature-dependent ESR method (210,211). At low temperature, the ESR spectrum shows an anisotropic triplet-triplet, indicating that it is very close to the rigid limit in the ESR time scale (average rotational correlation time, $>10^{-6}$ s). Motional effects on the spectra become pronounced with increasing temperature, resulting in essentially an isotropic and equally spaced hyperfine triplet. The lineshape simulations were done by adopting the Brownian rotational diffusion model in order to evaluate the associated (average) rotational correlation time, $\tau_{\bar{R}}$, and its degree of anisotropy, $N = \tau_{R_\parallel}/\tau_{R_\perp}$. It was found that the value of $\tau_{\bar{R}}$ decreased from 1.7×10^{-9} (230 K) to 7.5×10^{-10} s (325 K) with increasing temperature, and that N was very close to 1 ($N = 1.25$) in the motional narrowing region. The Arrhenius plots gave 5.9 kJ mol^{-1} for the activation energy, which was evaluated for the nearly isotropic rotational diffusion of NO_2 in Na-FAU(X) zeolite.

The ESR lineshapes of NO_2 adsorbed on Na-MOR and Na-MFI cannot be simulated adequately using the Brownian rotational diffusion model (212,213). Instead, the best agreement with the experimental lineshapes are obtained with a Heisenberg type of spin exchange. Therefore, the main cause for the reversible spectral change with temperature is due to the Heisenberg type of exchange. This conclusion agrees with the observation that spectral resolution is lower in samples exposed to high NO_2 pressure (13.3 kPa) than those exposed to low pressure (0.13–1.33 kPa). Rotational diffusion may occur to some extent but its effect on the lineshapes is hidden by the dominating exchange interaction. Recently, analysis utilizing the Heisenberg spin exchange model was improved by adopting a rate distribution (214). The dynamics of NO_2 is strongly dependent on the type of zeolite (215), Si/Al ratio (213), and type of cation (216). The temperatures at which the rigid limit spectra were observed were dependent on the type of zeolite channel structure as: MFI (<3 K) $\approx$ BEA (<4.2 K) $<$ FER (<20 K) $<$ LTL (30 K) $<$ MOR (77 K). The Heisenberg spin exchange rate increased in the following order, MFI $\approx$ BEA $>$ FER $>$ LTL $>$ MOR (215). From this order the following can be concluded: (a) the rate is faster in multiple-channel structural zeolites (MFI, BEA, and FER) than in the single-channel zeolites (LTL and MOR), and (b) in zeolites of similar channel structure, the exchange rate is proportional to the channel size. Provided that the order prevails also at high temperature, this indicates that NO removal in zeolites may be a diffusion-controlled reaction. Unfortunately, a study dealing with NO_2 diffusion was not applied for the catalysts active for NO reduction, such as Cu-MFI and transition metal ion–exchanged zeolite. However, it is expected that it will be done in the near future.

VI. CONCLUSIONS

In this chapter, the removal of nitrogen monoxide over metal ion–exchanged zeolites is introduced. It is widely accepted that copper zeolites show the best catalytic activity for NO decomposition, and that they are useful models for investigation of the fundamental aspects of the interaction chemistry and surface transformation of nitrogen oxides. The discovery of HC-SCR over copper zeolites has been one of the major developments in "environmental catalysis" in the last century. In general, environmental catalysts, have to work under severe conditions, wide temperature ranges, high space velocities, low concentrations of target materials, high concentrations of coexisting gases and poisons, and considerable changes in the reaction conditions. Therefore, environmental catalysts must have very high activities, selectivities, and durabilities. We expect much progress in the near future, both with respect to the development of

environmentally benign technology and in the scientific understanding of the catalytic action of deNOx.

REFERENCES

1. R J Farrauto, C H Bartholomew. Fundamentals of Industrial Catalytic Processes. London: Blackie, 1997, pp 580–666.
2. G Centi, S Perathoner. Catal Today 53:11, 1999.
3. A Foruny, J Font, A Fabregat. Appl Catal B 19:165, 1998; F E Hancock. Catal Today 53:3, 1999; F Luck. Catal Today 53:81, 1999; R Ukropec, B F M Kuster, J C Schoulten, R A van Santen. Appl Catal B 23:45, 1999.
4. J -M Herrmann. Catal Today 53:115, 1999; B Bems, F C Jentoft, R Schlögl. Appl Catal B 20:155, 1999; T Mori, J Suzuki, K Fujimoto, M Watanabe, Y Hasegawa. Appl Catal B 23:283, 1999; D Chen, A K Ray. Appl Catal B 23:143, 1999; K -H Wang, Y Hsieh, M -Y Chou, C -Yu Chang, Appl Catal B 21:1, 1999.
5. N -Y Topsoe. Infrared Spectroscopic Investigation on Environmental DeNOx and Hydrotreating Catalysts. Lyngby, Denmark: Haldor Topsoe Res Lab., 1998. pp 121–210.
6. J Widdershoven, F Pischinger, G Lepperhof. SAE paper 860013, Detroit, 1996.
7. Y Teraoka, K Nakano, S Kagawa, W Shangguan. Appl Catal B 5:L181, 1995; J C Summers, S Van Houtte, D Psaras. Appl Catal B 10:139, 1996; P Ciambelli, V Palma, P Russo, S Vaccaro. Appl Catal B 22:L5, 1999; J Oi-Uchisawa, A Obuchi, A Ogata, R Enomoto, S Kushiyama. Appl Catal B 21:9, 1999.
8. C A Querini, M A Ulla, F Requejo, J Soria, U A Sedrán, E E Miró. Appl Catal B 14:323, 1997; C A Querini, L M Cornaglia, M A Ulla, E E Miro. Appl Catal B 20:165, 1999.
9. G M Rusch. Drug Chem Toxicol 23:27–40, 2000.
10. S Imamura, T Shiomi, S Ishida, K Utani, H Jindai. Ind Eng Che Res 29:1758, 1990; J Burdeniu, R H Crabtree. Science 271:340, 1996; G -L Li, T Ishihara, Y Moro-oka, Y Takita. Appl Catal B 9:239, 1996; X Fu, W A Zellner, Q Yang, M A Anderson. J Catal 168:482, 1997; Y Takita, G -L Li, R Matsuzaki, H Wakamatsu, H Nishiguchi, Y Moro-oka, T Ishihara. Chem Lett 13, 1997; C F Ng, S Shan, S Y Lai. Appl Catal A 16:209, 1998.
11. B Coq, F Figuéras, S Hub, D Tournigant. J Phys Chem 99:11159, 1995; B Dhandapani, S T Oyama. Catal Lett 35:353, 1995; Z Karpinski, D Early, J L d'Itri. J Catal 164:378, 1996; B S Ahn, S C Lee, D J Moon, B G Lee. J Mol Catal A 106:83, 1996; S P Scott, M Sweetman, J Thomson, A G Fitzgerald, E J Sturrock. J Catal 168:501, 1997; E J A X van de Sandt, A Wiersma, M Makkee, H van Bekkum, J A Moulijn. Catal Today 35:163, 1997; F H Ribeiro, C A Gerken, G A Somorjai. Catal Lett 45:149, 1997; W Juszczyk, A Malinowski, Z Karpinski. Appl Catal A General 166:311, 1998.
12. Y Takita, H Hamada, T Ishihara, Y Mizuhara. J Chem Soc Jpn 5:584, 1991; A R Suzdorf, S V Morozov, N N Anshits, S I Tsiganova, A G Anshits. Catal Lett 29:49, 1994; J Estellé, J Ruz, Y Cesteros, R Fernández, P Salagre, F Medina, J E Sueiras. J Chem Soc, Faraday Trans 92:2811, 1996; T Mori, W Ueda, J Morikawa. Catal Lett 38:73, 1996; A Morato, C Alonso, F Medina, P Salagre, J E Sueiras, R Terrado, A Giralt. Appl Catal B 23:175, 1999.
13. M Iwamoto, S Yokoo, K Sakai, S Kagawa. J Chem Soc, Faraday Trans 1, 77:1629, 1981.
14. (a) M Iwamoto. Stud Surf Sci Catal 54:121, 1990; M Iwamoto, H Hamada. Catal Today 10:57, 1991; M Iwamoto, N Mizuno. J Automobile Eng 207:23, 1993; M Iwamoto. Stud Surf Sci Catal 84:1395, 1994; M Iwamoto. Catal Today 29:29, 1996; (b) A Fritz, V Pitchon. Appl Catal B 13:1, 1997; (c) H Akama, H Kanesaki, S Yamamoto, K Matsumoto. Jidoushagijutu 54:77, 2000.
15. M Iwamoto, H Furukawa, Y Mine, F Uemura, S Mikuriya, S Kagawa. J Chem Soc, Chem Commun 1272, 1986.
16. Y Li, W K Hall. J Catal 129:202, 1991.
17. M Iwamoto, H Yahiro, Y Yu-u, S Shundo, N Mizuno. Shokubai 32:430, 1990.

18. W Held, A Konig, T Richter, L Puppe. SAE Trans, Section 4 No 900 469:209, 1990.
19. W Zhang, H Yahiro, N Mizuno, J Izumi, M Iwamoto. Langmuir 9:2337, 1993.
20. W Zhang, H Yahiro, J Izumi, M Iwamoto. J Chem Soc, Faraday Trans 91:767, 1995.
21. W Zhang, H Yahiro, N Mizuno, J Izumi, M Iwamoto. J Mater Sci Lett 12:1197, 1993; W Zhang, M Jia, J Yu, T Wu, H Yahiro, M Iwamoto. Chem Mater 11:920, 1999.
22. For example, H Arai, M Machida. Catal Today 22:97, 1994; M Machida. Catalysis 15:73, 2000.
23. D Barthomeuf. J Phys Chem 83:249, 1979.
24. Y Okamoto, M Ogawa, A Maezawa, T Imanaka. J Catal 112:427, 1988.
25. M C Kung, H H Kung. Catal Rev 27:425, 1985.
26. K I Hadjiivanov. Catal Rev 42:71, 2000.
27. M Iwamoto, H Yahiro, N Mizuno, W -X Zhang, Y Mine, H Furukawa, S Kagawa. J Phys Chem 96:9360, 1992.
28. J Valyon, W K Hall. J Phys Chem 97:1204, 1993.
29. J Pearce, D Sherwood, M Hall, J Lunsford. J Phys Chem 84:3215, 1980; K A Windhorst, J H Lunsford. J Am Chem Soc 97:1407, 1975.
30. A Aylor, L Lobree, J Reimer, A T Bell. J Catal 170:390, 1997.
31. K Hadjiivanov, H Knozinger, B Tsyntsarski, L Dimitrov. Catal Lett 62:35, 1999.
32. K Segawa, Y Chen, J E Kubsh, W N Delgass, J A Dumesic, W K Hall. J Catal 76:112, 1982.
33. Y Li, T L Slager, J N Armor. J Catal 150:388, 1994.
34. T Tabata, H Ohtsuka, L M F Sabatino, G Bellussi. Micropor Mesopor Mater 21:517, 1998.
35. P H Kasai, R J Bishop, Jr, D McLeod, Jr. J Phys Chem 82:279, 1978.
36. H Niessner, I Burkhardt, D Gutshick. J Chem Soc, Faraday Trans 86:2329, 1990.
37. L H Lobree, A W Aylor, A J Reimer, A T Bell. J Catal 181:189, 1999.
38. J Rask, F Solymosi. J Chem Soc, Faraday Trans 1 80:1841, 1984.
39. K Hadjiivanov. Micropor Mesopor Mater 24:41, 1998.
40. C C Chao, J H Lunsford. J Phys Chem 78:1174, 1974.
41. S Qiu, R Ohnishi, M Ichikawa. J Phys Chem 98:2719, 1994.
42. T Salama, R Ohnishi, T Shido, M Ichikawa. J Catal 162:169, 1996.
43. C E Dinerman, G E Ewing. J Chem Phys 53:626, 1970.
44. F A Cotton, G Wilkinson. Advanced Inorganic Chemistry, 4th ed. New York: Wiley, 1980, p 697.
45. C C Chao, J H Lunsford. J Am Chem Soc 93:71, 1971.
46. K Hadjiivanov, J Saussey, J L Freysz, J C Lavalley. Catal Lett 52:103, 1998.
47. V I Pârvulescu, P Oelker, P Grange, B Delmon. Appl Catal B 16:1, 1998.
48. E Giamello, D Murphy, G Magnacca, C Morterra, Y Shioya, T Nomura, M Anpo. J Catal 136:510, 1992.
49. T Beutel, B Adelman, W M H Sachtler. Appl Catal B 9:L1, 1996.
50. J Szanyi, M T Paffett. J Catal 164:232, 1996.
51. J Dedecek, Z Sobalik, Z Tvaruzkova, D Kaucky, B Wichterlová. J Phys Chem 99:16327, 1995.
52. V I Pârvulescu, P Grange, B Delmon. J Phys Chem B 101:6933, 1997.
53. A Aylor, S Larsen, J Reimer, A T Bell. J Catal 157:569, 1995.
54. H Jang, W K Hall, J d'Itri. J Phys Chem 100:9416, 1996.
55. M Anpo, M Matsuoka, Y Shioya, H Yamashita, E Giamello, C Morterra, M Che, H H Patterson, S Webber, S Ouellette, M A Fox. J Phys Chem 98:5744, 1994.
56. C Naccache, M Che, Y Ben Taarit. Chem Phys Lett 13:109, 1972.
57. C C Chao, J H Lunsford. J Phys Chem 76:1546, 1972.
58. Z Sojka, M Che, E Giamello. J Phys Chem B 101:4831, 1997.
59. B L Trout, A K Chakraborty, A T Bell. J Phys Chem 100:17582, 1996.
60. Y Yokomichi, T Yamabe, H Ohtsuka, T Kakumoto. J Phys Chem 100:14424, 1996.
61. G Spoto, S Bordiga, D Scarano, A Zecchina. Catal Lett 13:39, 1992.
62. M Iwamoto, H Yahiro, N Mizuno. J Chem Soc Jpn 574, 1991.
63. P A Jacobs, W De Wilde, R A Shoonheydt, J B Uytterhoeven. Trans Faraday Soc 5:1221, 1976.

64. Y Li, J N Armor. Appl Catal B 2:239, 1993. Y Li, J N Armor. J Catal 150:376, 1994.
65. C Y Zhu, C W Lee, P J Chong. Zeolites 17:483, 1996.
66. B Djonev, B Tsyntsarski, D Klissurski, K Hadjiivanov. J Chem Soc, Faraday Trans 93:4055, 1997.
67. J H Lunsford. J Phys Chem 72:4163, 1968.
68. C L Gardner, M A Weinberger. Can J Chem 48:1317, 1970.
69. P H Kasai, R J Bishop, Jr. J Am Chem Soc 94:5560, 1972.
70. P H Kasai, R J Bishop, Jr. Zeolite Chemistry and Catalysis (J A Rabo, ed.). ACS Monograph 171, Washington, DC, 1976, p 350.
71. H Yahiro, A Lund, R Aasa, N P Benetis, M Shiotani. J Phys Chem A 104:7950, 2000.
72. H Yahiro, N P Benetis, A Lund, M Shiotani. Stud Surf Sci Catal 135:348, 2001.
73. D Biglino, H Li, R Erikson, A Lund, H Yhairo, M Shiotani. Phys Chem Chem Phys 1:2887, 1999.
74. R M Barrer. J Colloid Int Sci 21:415, 1966.
75. A Gutsze, M Plato, H Karge, F Witzel. J Chem Soc, Faraday Trans 92:2495, 1996.
76. A Pöppl, T Rudolf, D Michel. J Am Chem Soc 120:4879, 1998; A Pöppl, T Rudolf, P Manikandan, D Goldfarb. J Am Chem Soc 122:10194, 2000.
77. P H Kasai, R M Gaura. J Phys Chem 86:4257, 1982.
78. H Yahiro, K Kurohagi, G Okada, Y Itagaki, M Shiotani, A Lund. Phys Chem Chem Phys 4:4255, 2002.
79. A Volodin, D Biglino, Y Itagaki, M Shiotani, A Lund. Chem Phys Lett 323:165, 2000.
80. D Biglino, M Bonora, A Volodin, A Lund. Chem Phys Lett 349:511, 2001.
81. M Iwamoto, H Yahiro, Y Mine, S Kagawa. Chem Lett 213, 1989.
82. M Iwamoto, H Yahiro, K Tanda, N Mizuno, Y Mine, S Kagawa. J Phys Chem 95:3727, 1991.
83. Y Li, W K Hall. J Phys Chem 94:6145, 1990.
84. M Iwamoto, H Yahiro, K Tanda. Stud Surf Sci Catal 44:219, 1988.
85. M Iwamoto, M Nakamura, H Nagano, T Seiyama. J Phys Chem 86:153, 1982.
86. Y Teraoka, C Tai, H Ogawa, H Furukawa, S Kagawa. Appl Catal A 200:167, 2000.
87. B Ganemi, E Björnbom, J Paul. Appl Catal B 17:293, 1998; B Ganemi, E Björnbom, B Demirel, J Paul. Micropor Mesopor Mater 38:287, 2000.
88. J Dedecek, J Cejka, B Wichterlová. Appl Catal B 15:233, 1998.
89. Z Schay, L Guczi, Zs Koppány, I Nagy, A Beck, V Samuel, M K Dongare, D P Sabde, S G Hegde, A V Ramaswamy. Catal Today 54:569, 1999.
90. S Kagawa, H Ogawa, H Furukawa, Y Teraoka. Chem Lett 407, 1991; Y Zhang, M Flytzani-Stephanopoulos. J Catal 164:131, 1996.
91. Y Chang, J G McCarty. J Catal 178:408, 1998.
92. G K Boreskov. Discuss Faraday Soc 41:263, 1966; H Hamada, Y Kintaichi, M Sasaki, T Ito. Chem Lett 1069, 1990; P W Park, J K Kil, H H Kung, M C Kung. Catal Today 42:51, 1998.
93. H Shimada, S Miyama, H Kuroda. Chem Lett 1797, 1988.
94. T Uchijima. Hyomen 18:132, 1987; Y Teraoka, H Fukuda, S Kagawa. Chem Lett 1, 1990; H Yasuda, N Mizuno, M Misono. J Chem Soc Chem Commun 1094, 1990.
95. S Xie, M P Rosynek, J H Lunsford. J Catal 188:24, 1999.
96. T E Green, C N Hinshelwood. J Chem Soc 128:1708, 1926. P W Bachman, G B Tayler. J Phys Chem 33:447, 1929. J Zawadski, G Perlinsky. Compt Rend 198:260, 1934. R R Sakaida, R G Rinker, Y L Wang, W H Corcoran. AIChE J 7:658, 1961. M Shelef, K Otto, H Gandhi. Atmos Environ 3:107, 1969. A Amimazmi, J E Benson, M Boudart. J Catal 30:55, 1973. A Amimazmi, M Boudart. J Catal 39:383, 1975. S Pancharatnum, K J Lim, D M Mason. Chem Eng Sci 30:781, 1975. K Sakata, T Uchijima, Y Yoneda. Nippon Kagaku Kaishi 791, 1978.
97. S S C Chuang, C -D Tan. J Phys Chem B 101:3000, 1997.
98. M Iwamoto. Stud Surf Sci Catal 130:23, 2000.
99. M Shelef. Chem Rev 95:209, 1995. J N Armor. Catal Today 26:99, 1995.
100. R A Schoonheydt, L J Vondamme, P A Jacobs, J B Uytterhoeven. J Catal 43:292, 1976.

101. M Iwamoto, N Mizuno, H Yahiro, T Yoshioka. New Developments in Ion Exchange. Tokyo: Kodansha, 1991, p 407.
102. J Vaylon, W K Hall. Catal Lett 19:109, 1993.
103. G Centi, S Perathoner. Appl Catal A 132:179, 1995.
104. Y Kuroda, A Kotani, H Maeda, H Moriwaki, T Morimoto, M Nagao. J Chem Soc, Faraday Trans 88:1583, 1992.
105. M Iwamoto, H Yahiro, Y Torikai, T Yoshioka, N Mizuno. Chem Lett 1967, 1990.
106. H G Karge, H K Beyer. Stud Surf Sci Catal 69:43, 1991. H G Karge. Zeolite Microporous Solids: Synthesis, Structure, and Reactivity (E Derouane, C Naccache, F R Riberio, eds.). Dordrecht: Kluwer Academic, 1992, p 273.
107. G Spoto, A Zecchina, S Bordiga, G Ricchiardi, G Martra, G Leofanti, G Petrini. Appl Catal B 3:151, 1994.
108. M Iwamoto, N Mizuno, H Yahiro. J Jpn Petrol Inst 34:375, 1991.
109. M Iwamoto, H Yahiro. Catal Today 22:5, 1994.
110. G J Millar, A Canning, G Rose, B Wood, L Trewartha, I D R Mackinnon. J Catal 183:169, 1999.
111. D -J Liu, H J Robota. Catal Lett 21:291, 1993. D -J Liu, H J Robota. Appl Catal B 4:155, 1994.
112. Y Hoshino, M Iwamoto. Chem Lett 631, 1996. M Iwamoto, Y Hoshino. Inorg Chem 35:6918, 1996.
113. J Valyon, W K Hall. J Phys Chem 97:7054, 1993.
114. J Sarkany, J L d'Itri, W M H Sachtler. Catal Lett 16:241, 1992.
115. G D Lei, B J Adelman, J Sarkany, W M H Sachtler. Appl Catal B 5:245, 1995.
116. N C N A Carvalho, F B Passos, M Schmal. Appl Catal A 193:265, 2000.
117. S C Larsen, A W Aylor, A T Bell, J A Reimer. J Phys Chem 98:11533, 1994.
118. G Moretti, C Dossi, A Fusi, S Recchia, R Psaro. Appl Catal B 20:67, 1999.
119. J Sarkany, W M H Sachtler. Zeolites 14:7, 1994.
120. G Moretti. Catal Lett 23:135, 1994.
121. M C Campa, V Indovina, G Minelli, G Moretti, I Pettiti, P Porta, A Piccio. Catal Lett 23:141, 1994.
122. K C C Kharas. Appl Catal B 2:207, 1993.
123. D C Sayle, C Richard, A Catlow, M -A Perrin, P Nortier. Micropor Mesopor Mater 20:259, 1998.
124. B Wichterlová, J Dedecek, A Vondrová. J Phys Chem 99:1065, 1995.
125. M V Konduru, S S C Chuang. J Catal 187:436, 1999.
126. J Valyon, W K Hall. Stud Surf Sci Catal 75:1333, 1993.
127. M V Konduru, S S C Chuangs. J Phys Chem 103:5802, 1999.
128. J Dedecek, B Wichterlová. J Phys Chem 98:5721, 1994. B Wichterlová, Z Sobalik, A Vondrová. Catal Today 29:149, 1996. B Wichterlová, J Dedecek, Z Sobalik, A Vondrová, K Klier. J Catal 169:194, 1997. J Dedecek, B Wichterlová. J Phys Chem B 101:10233, 1997. B Wichterlová, Z Sobalik, J Dedecek. Catal Today 38:199, 1997. Z Sobalik, J Dedecek, I Ikonnikov, B Wichterlová. Micropor Mesopor Mater 21:525, 1998. Z Sobalik, Z Traruzkova, B Wichterlová. J Phys Chem B 102:1077, 1998.
129. J Dedecek, B Wichterlová. Phys Chem Chem Phys 1:629, 1999.
130. Y Kuroda, S Konno, H Maeda, Y Yoshikawa. Jpn J Appl Phys 32:493, 1993. Y Kuroda, Y Yoshikawa, S Konno, H Hamano, H Maeda, R Kumashiro, M Nagao. J Phys Chem 99:10621, 1995. Y Kuroda, H Maeda, Y Yoshikawa, R Kumashiro, M Nagao. J Phys Chem B 101:1312, 1997. Y Kuroda, S Konno, Y Yoshikawa, H Maeda, Y Kubozono, H Hamano, R Kumashiro, M Nagao. J Chem Soc, Faraday Trans 93:2125, 1997. Y Kuroda, Y Yoshikawa, R Kumashiro, M Nagao. J Phys Chem B 101:6497, 1997. R Kumashiro, Y Kuroda, M Nagao. J Phys Chem B 103:89, 1999. Y Kuroda, Y Yoshikawa, S Emura, R Kumashiro, M Nagao. J Phys Chem B 103:2155, 1999. Y Kuroda, T Mori, Y Yoshikawa, S Kittaka, R Kumashiro, M Nagao. Phys Chem Chem Phys 1:3807, 1999. Y Kuroda, R Kumashiro, A Itadani, M Nagao, H Kobayashi. Phys Chem Chem Phys 3:1383, 2001.

131. Y Kuroda, Y Kumashiro, T Yoshimoto, M Nagao. Phys Chem Chem Phys 1:649, 1999.
132. D Nachtigallova, P Nachtigall, M Sierka, J Sauer. Phys Chem Chem Phys 1:2019, 1999.
133. B R Goodman, K C Hass, W F Schneider, J B Adams. Catal Lett 56:183, 1998. B R Goodman, K C Hass, W F Schneider, J B Adams. J Phys Chem B 103:10452, 1999.
134. M D Amiridis, T Zhang, R J Farrauto. Appl Catal B 10:203, 1996.
135. V Yentekakis, M Konsolakis, R M Lambert, N Macleod, L Nalbantian. Appl Catal B 22:123, 1999. R Burch, P Fornasiero, B W L Southward. J Catal 182:234, 1999. R Burch, J A Sullivan. J Catal 182:489, 1999. R Burch, A A Shestov, J A Sullivan. J Catal 182:497, 1999. M Xin, I C Hwang, D H Kim, S I Cho, S I Woo. Appl Catal B 21:183, 1999. R Burch, M D Coleman. Appl Catal B 23:115, 1999. E Joubert, T Bertin, J C Menezo, J Barbier. Appl Catal B 23:L83, 1999. F Garin, P Girard, S Ringler, G Maire, N Davias. Appl Catal B 20:205, 1999. S Ringler, P Girard, G Maire, S Hilaire. Appl Catal B. 20:219, 1999. D K Captain, M D Amiridis. J Catal 184:377, 1999. V Pitchon, A Fritz. J Catal 186:64, 1999.
136. J Mitome, G Karakas, K A Bryan, U S Ozkan. Catal Today 42:3, 1998. M Ogura, M Hayashi, S Kage, M Matsukata, E Kikuchi. Appl Catal B 23:247, 1999. H Ohtsuka, T Tabata. Appl Catal B 21:133, 1999. A M Pisanu, C E Gigola. Appl Catal B 20:179, 1999. K Almusaiteer, S S C Chuang. J Catal 184:189, 1999. M Schmal, M A S Baldanza, M A Vannice. J Catal 185:138, 1999.
137. E A Efthimiadis, S C Christoforou, A A Nikolopoulos, I A Vasalos. Appl Catal B 22:91, 1999. C S Gopinath, F Zaera. J Catal 186:387, 1999.
138. H Jen. Catal Today 42:37, 1998. M Haneda, Y Kintaichi, M Inaba, H Hamada. Catal Today 42:127, 1998. Z Li, M F-Stephanopoulos. J Catal 182:313, 1999. F C Meunier, J R H Ross. Appl Catal B 24:23, 2000.
139. N Okazaki, S Tsuda, Y Shiina, A Tada, M Iwamoto. Chem Lett 429, 1998. T Nanba, A Uemura, A Ueno, M Haneda, H Hamada. Bull Chem Soc Jpn 71:2331, 1998. D Tapanee, P Piyasan, T Inui. Catal Lett 61:77, 1999. J Desai, V I Kovalchuk, E A Lombardo, J L d'Itri. J Catal 184:396, 1999. Y G Kim, Y C Kim, S B Hong, M H Kim, Y P Kim, Y S Uh. Catal Lett 57:179, 1999. Y -F Chang, A Sanjurjo, J G McCarty, G Krishnan, B Woods, E Wachsman. Catal Lett 57:187, 1999.
140. Y Traa, B Burger, J Weikamp. Micropor Mesopor Mater 30:3, 1999.
141. S Sato, Y Yu-u, H Yahiro, N Mizuno, M Iwamoto. Appl Catal 70:L1, 1991.
142. F -S Xiao, W Zhang, M Jia, Y Yu, C Fang, Guoxingbatu, S Zheng, S Qiu, R Xu. Catal Today 50:117, 1999.
143. C Torre-Abreu, C Henriques, F R Riberio, G Delahay, M F Ribeiro. Catal Today 54:407, 1999.
144. A Corma, V Fornés, E Palomares. Appl Catal B 11:233, 1997.
145. G Delahay, B Coq, L Broussous. Appl Catal B 12:49, 1997.
146. F S Azad, D Zhang. Catal Today 68:161, 2001.
147. Y Li, J N Armor. Appl Catal B 1:L31, 1992.
148. K Yogo, S Tanaka, M Ihara, T Hishiki, E Kikuchi. Chem Lett 1025, 1992.
149. Y Nishizaka, M Misono. Chem Lett 1295, 1993.
150. M Konno, T Chikahisa, T Murayama, M Iwamoto. SAE Paper 920091, 1, 1992.
151. M Iwamoto, H Yahiro, S Shundo, Y Yu-u, N Mizuno. Appl Catal 69:L15, 1991.
152. T Ishihara, M Kagawa, F Hamada, Y Takita. Stud Surf Sci Catal 84:1493, 1994.
153. A E Palomares, F Márques, S Valencia, A Corma. J Mol Catal A 162:175 2000.
154. K C C Kharas, H J Robota, D J Liu. Appl Catal B 2:225, 1993.
155. T Tabata, M Kokitsu, O Okada, T Nakayama, T Yasumatsu, H Sakane. Stud Surf Sci. Catal 88:409, 1994.
156. J Y Yan, G D Lei, W M H Sachtler, H H Kung. J Catal 161:43, 1996.
157. S Matsumoto, K Yokota, H Doi, M Kimura, K Sekizawa, S Kasahara. Catal Today 22:127, 1994.
158. T Tanabe, T Iijima, A Koiwai, J Mizuno, K Yokota, A Isogai. Appl Catal B 6:145, 1995.
159. A V Kucherov, A A Slinkin, S S Goryashenko, K I Slovetskaja. J Catal 118:459, 1989. A V Kucherov, C P Hubbard, M Shelef. J Catal 157:603, 1995. A V Kucherov, J L Gerlock, H -W Jen, M Shelef. J Catal 152:63, 1995.

160. M Iwamoto, J Wang, K M Sperati, T Sajiki, M Misono. Chem Lett 1281, 1997.
161. T Inui, S Iwamoto, K Matsuba, Y Tanaka, T Yoshida. Catal Today 26:23, 1995.
162. A V Kucherov, C P Hbbard, T N Kucherova, M Shelef. Appl Catal B 7:285, 1996. J Y Yan, W M H Sachtler, H H Kung. Catal Today 33:279, 1997. P Budi, R F Howe. Catal Today 38:175, 1998. M Guyon, V Le Chanu, P Gilot, H Kessler, G Prado. Stud Surf Sci Catal 116:297, 1998. W E J van Kooten, J Kaptein, C M van den Bleek, H P A Calis. Catal Lett 63:227, 1999.
163. R L Keiski, H Raisamen, M Harkonen, T Maunnula, P Niemisto. Catal Today 27:85, 1996.
164. T Kesen, Y Kawashima, H Akama, M Kamikubo. Shokubai 39:119, 1997.
165. R Burch, P J Millington. Appl Catal B 2:101, 1993. R Burch, P J Millington, A P Walker. Appl Catal B 4:65, 1994. R Burch, S Scire. Catal Lett 27:177, 1994. T Inui, S Iwamoto, S Kojo, T Yoshida. Catal Lett 13:87, 1992. T Inui, T Hirabayashi, S Iwamoto. Catal Lett 27:267, 1994. T Inui, S Iwamoto, S Kojo, S Shimizu, T Hirabayashi. Catal Today 22:41, 1994. B K Cho. J Catal 155:184, 1995.
166. E V Rebrov, A V Simakov, N N Sazonova, E S Stoyanov. Catal Lett 58:107, 1999.
167. M H Kim, I-S Nam, Y G Kim. Appl Catal B 6:297, 1995. M Iwamoto, H Takeda. Catal Today 27:71, 1996. H Hamada, Y Kintaichi, M Sasaki, T Ito. Appl Catal 70:L15, 1991. E Kikuchi, K Yogo. Catal Today 22:73, 1994. T E Hoost, K A Laframboise, K Otto. Appl Catal B 7:79, 1995. D B Lukyanov, G Still, J L d'Itri, W K Hall. J Catal 153:265, 1995. A D Cowan, R Dumpelmann, N W Cant. J Catal 151:356, 1995. H Kato, C Yokoyama, M Misono. Catal Lett 47:189, 1997. M Shelef, C N Montreuil, H W Jen. Catal Lett 26:277, 1994. K A Bethke, C Li, M C Kung, H H Kung. Catal Lett 31:287, 1995. M Guyon, V L Chanu, P Gilot, H Kessler, G Prado. Appl Catal B 8:183, 1996. K Hadjiivanov, D Klissurski, G Ramis, G Busca. Appl Catal B 7:251, 1996. H Takeda, M Iwamoto. Catal Lett 38:21, 1996. S A Beloshapkin, E A Paukshtis, V A Sadykov. J Mol Catal A 158:355, 2000.
168. B J Adelman, T Beutel, G Lei, W M H Sachtler. Appl Catal B 11:L1, 1996.
169. H -Y Chen, T Voskoboinikov, W M H Sachtler. J Catal 186:91, 1999.
170. X Feng, W K Hall. Catal Lett 41:45, 1996.
171. X Feng, W K Hall. J Catal 166:368, 1997.
172. H -Y Chen, W M H Sachtler. Catal Today 42:73, 1998.
173. H -Y Chen, W M H Sachtler. Catal Lett 50:125, 1998.
174. M Kögel, V H Sandoval, W Schwieger, A Tissler, T Turek. Catal Lett 51:23, 1998.
175. W K Hall, X Feng, J Dumesic, R Watwe. Catal Lett 52:135, 1998.
176. H -Y. Chen, X Wang, W M H Sachtler. Appl Catal A 194:159, 2000.
177. W N Delgass, R L Garten, M Boudart. J Phys Chem 73:2970, 1969. J Chem Phys 50:4603, 1969.
178. C Pophal, T Yago, K Tanabe, K Segawa. Catal Lett 44:271, 1997. Appl Catal B 16:177, 1998.
179. K Lazar, G P Borbély, H K Beyer, H G Karge. Stud Surf Sci Catal 91:145, 1995.
180. J Varga, Á Fudala, J Halász, G Schöbel, I Kirisci. Stud Surf Sci Catal 94:665, 1995.
181. M Kögel, R Monnig, W Schwieger, A Tissler, T Turek. J Catal 182:470, 1999.
182. H -T Lee, H -K Rhee. Catal Lett 61:71, 1999.
183. L J Lobree, I -C Hwang, J A Reimer, A T Bell. Catal Lett 63:233, 1999.
184. M Lezcano, V I Kovalchuk, J L d'Itri. Kinetics and Catal 42:104, 2001.
185. T V Voskoboinikov, H -Y Chen, W M H Sachtler. Appl Catal B 19:279, 1998. T V Voskoboinikov, H -Y Chen, W M H Sachtler. J Mol Catal A 158:155, 2000. H -Y Chen, El-M El-Malki, X Wang, R A van Santen, W M H Sachtler. J Mol Catal A 162:159, 2000.
186. P Marturano, L Drozdova, A Kogelbauer, R Prins. J Catal 192:236, 2000.
187. H -Y. Chen, T Voskoboinikov, W M H Sachtler. J Catal 180:171, 1998. Catal Today 54:483, 1999. L J Lobree, I -C Hwang, J A Reimer, A T Bell. J Catal 186:242, 1999. X Wang, H Y-Chen, W M H Sachtler. J Catal 197:281, 2001.
188. O Y Liu, N W Cant, M Kogel, T Turek. Catal Lett 63:241, 1999.
189. F Kapteijin, J R Mirasol, J A Moulijn. Appl Catal B 9:25, 1996.

190. M Ogura, S Hiromoto, E Kikuchi. Chem Lett 1135, 1995. E Kikuchi, M Ogura, N Aratani, Y Sugiura, S Hiromoto, K Yogo. Catal Today 27:35, 1996.
191. C Yokoyama, M Misono. Catal Lett 29:1, 1994.
192. N Takahashi, H Shinjoh, T Iijima, T Suzuki, K Yamazaki, K Yokota, H Suzuki, N Miyoshi, S Matsumoto, T Tanizawa, T Tanaka, S Tateishi, K Kasahara. Catal Today 27:63, 1996.
193. M Iwamoto, A M Hernandez, T Zengyo. J Chem Soc, Chem Commun 37, 1997. M Iwamoto, T Zengyo, A M Hernandez, H Araki. Appl Catal B 17:259, 1998.
194. M Machida, K Yasuoka, K Eguchi, H Arai. J Chem Soc Chem Commun 1165, 1990. K Eguchi, M Watanabe, S Ogata, H Arai. Bull Chem Soc Jpn 68:1739, 1995. K Eguchi, T Kondo, T Hayashi, H Arai. Appl Catal B 16:69, 1998.
195. E Fridell, M Skoglundh, B Westerberg, S Johansson, G Smedler. J Catal 183:196, 1999.
196. H Mahzoul, J F Brilhac, P Gilot. Appl Catal B 20:47, 1999.
197. W Bögner, M Krämer, B Krutzsch, S Pischinger, D Voigtländer, G Wenninger, F Wirbeleit, M S Brogan, R J Brisley, D E Webster. Appl Catal B 7:153, 1995.
198. S Hodjati, P Bernhardt, C Petit, V Pitchon, A Kiennemann. Appl Catal B 19:209 & 221, 1998.
199. N Fekete, R Kemmler, D Voigtländer, B Krutzsch, E Zimmer, G Wenninger, W Strehlau, J A A Van Der Tillaart, J Leyrer, E S Lox, W Mülller. SAE Paper 970746, 1997.
200. N Miyoshi, S Matsumoto, K Katoh, T Tanaka, J Harada, N Takahashi, K Yokota, M Sugiura, K Kasahara. SAE Paper 950809, 1995.
201. P Engstrom, A Amberntsson, M Skoglundh, E Fridell, G Smedler. Appl Catal B 22:L241, 1999.
202. J Guo, M Konno, T Chikahisa, T Murayama, M Iwamoto. JSAE Review 16:21, 1995.
203. H K Shin, H Hirabayashi, H Yahiro, M Watanabe, M Iwamoto. Catal Today 26:13, 1995.
204. V I Pârvulescu, P Grange, B Delmon. Catal Today 46:233, 1998.
205. T Tabata, H Ohtsuka. Catal Lett 48:203, 1997.
206. A Shichi, A Satsuma, M Iwase, K Shimizu, S Komai, T Hattori. Appl Catal B 17:107, 1998.
207. A Shichi, K Katagi, A Satuma, T Hattori. Appl Catal B 24:97, 2000. A Shichi, A Satsuma, T Hattori. Appl Catal A 207:315, 2001.
208. T Ito, J Fraissard. J Chem Phys 76:5225, 1982.
209. E W Scharpf, R W Crecely, B C Gates, C Dybowski. J Phys Chem 90:9, 1986. T T P Cheung, C M Fu, S Wharry. J Phys Chem 92:5170, 1988. J A Ripmeester, C I Ratcliffe. J Phys Chem 94:7652, 1990. J Karger, H Pfeifer, T Wutscherk, S Ernst, J Weitkamp, J Fraissard. J Phys Chem 96:5059, 1992. F V-Maeder. J Phys Chem 98:4666, 1994. C J Jameson, A K Jameson, R E Gerald II, H -M Lim. J Chem Phys 103:8811, 1995.
210. H Yahiro, M Shiotani, J H Freed, M Lindgren, A Lund. Stud Surf Sci Catal 94:673, 1995.
211. S A Goldman, G V Bruno, C F Polnaszek, J H Freed. J Chem Phys 56:716, 1972.
212. M Nagata, H Yahiro, M Shiotani, M Lindgren, A Lund. Chem Phys Lett 256:27, 1996.
213. H Li, A Lund, M Lindgren, E Sagstuen, H Yahiro. Chem Phys Lett 271:84, 1997.
214. H Li, H Yahiro, M Shiotani, A Lund. J Phys Chem B 102:5641, 1998.
215. H Li, H Yahiro, K Komaguchi, M Shiotani, E Sagstuen, A Lund. Micropor Mesopor Mater 30:275, 1999.
216. H Yahiro, M Nagata, M Shiotani, M Lindgren, H Li, A Lund. Nukleonika 42:557, 1997.